NTNU
Norwegian University of
Science and Technology

Experimental Analysis for Next-Generation Wireless Sensor Networks

Hans Melby

Master of Science in Communication Technology
Submission date: June 2017
Supervisor: Pierluigi Salvo Rossi, IES
Co-supervisor: Indrakshi Dey, IES

Norwegian University of Science and Technology
Department of Electronic Systems

Preface

This thesis, carried out in the period between January and June 2017, concludes my study in the Communication Technology Master's program at the Department of Electronic Systems at NTNU in Trondheim, with a main emphasis on signal processing and communication. The topic of the thesis is the practical use of massive MIMO in wireless sensor networks, with a specific application scenario called decision fusion. No preparation project was done preceding this thesis.

I would like to extend a special thanks to professor Pierluigi Salvo Rossi and post-doctoral researcher Indrakshi Dey both for the opportunity to further explore this highly interesting field, and for all the cooperation and advice throughout the semester.

Also, a big thank you to my parents for all the support during all these years I've spent studying, and more recently, for help with proofreading and grammatical improvement suggestions.

Finally, a big thanks to the Communication Technology class of 2017 for all the great times throughout these last five years. You have provided me with friends and memories that are sure to last a lifetime.

Trondheim, June 2017
Hans Hellzen Melby

Abstract

Massive Multiple-Input-Multiple-Output (MIMO) has been outlined as one of the main technologies for achieving the potential in future communication networks. Its theoretical conception was approximately seven years ago, and since then, research activity has grown exponentially [1]. For this research to be commercialized, it is critical to find out how reality differs from theoretical results. This has now become possible with National Instruments' new Massive MIMO Application Framework, which aims at enabling researchers to rapidly prototype theoretical results in a practical scenario.

This thesis aims at using said application framework to understand the implications of using Massive MIMO in wireless sensor networks through a specific scenario called *Decision Fusion*, where the main principle is to combine data from multiple information sources to take a global decision about a physical event. In this case, the information sources are sensors measuring frequency spectrum activity, and the global decision is whether the spectrum is in use by other mobile units.

This work has produced an experiment model and real-world channel measurements that are in the process of being analyzed. The report outlines strengths and weaknesses of the model and suggests possible future work. All implementation files are in the attached folder.

Sammendrag

Massve Multiple-Input-Multiple-Output (MIMO) fremstår som en av hovedteknologiene for å utnytte potensialet i fremtidens kommunikasjonssystemer. Etter at teorien ble etablert for om lag syv år siden, har forskningsaktiviteten vokst eksponentielt [1]. For at nyere forskning skal få fotfeste i industrien, er det viktig å sammenlikne hvordan faktiske målinger skiller seg fra teoretiske resultater. Dette har nå blitt mulig takket være National Instruments sitt nye kombinerte program- og maskinvarerammeverk. Dette rammeverket gjør det mulig for forskere å raskt prototype teoretiske metoder i praktiske scenarioer.

Denne oppgaven bruker nevnt rammeverk i trådløse sensornettverk innen et spesifikt område som heter *Decision Fusion*, der hovedprinsippet er å kombinere data fra flere informasjonsskilder for å ta en avgjørelse angående en fysisk hendelse. I dette tilfellet er informasjonskildene sensorer som måler frekvensspekteraktivitet, og den fysiske hendelsen er om det gitte frekvensspekteret er i bruk av andre mobile enheter.

Oppgaven har produsert en eksperimentmodell og fysiske målinger som skal bli analysert for videre bruk (alle implementasjonsfiler ligger i den vedlagte mappen). Rapporten omtaler styrker og svakheter ved modellen og foreslår videre arbeid.

Table of Contents

List of Figures

Abbreviations

WSN	=	Wireless Sensor Network
MIMO	=	Multiple-Input-Multiple-Output
SISO	=	Single-Input-Single-Output
SIMO	=	Single-Input-Multiple-Output
UE	=	User Equipment
4G	=	4th Generation
5G	=	5th Generation
IMT	=	International Mobile Telecommunications
PSK	=	Phase Shift Keying
BPSK	=	Binary Phase Shift Keying
ROC	=	Receiver Operating Characteristic
DF	=	Decision Fusion
DFC	=	Decision Fusion Center
RF	=	Radio Frequency
NI	=	National Instruments
NTNU	=	Norwegian University of Science and Technology
TPR	=	True Positive Rate
FPR	=	False Positive Rate
USRP	=	Universal Software Radio Peripheral
SDR	=	Software Defined Radio
LabVIEW	=	Laboratory Virtual Instrument Engineering Workbench
BS	=	Base Station
MS	=	Mobile Station
CR	=	Cognitive Radio
PU	=	Primary User
SU	=	Secondary User
MRC	=	Maximum Ratio Combining
CSI	=	Channel State Information
MAC	=	Multiple Access Channel
FDM	=	Frequency Division Multiplexing
OFDM	=	Orthogonal Frequency Division Multiplexing
FIR	=	Finite Impulse Response
MA	=	Moving Average
LLR	=	Log-Likelihood Ratio
PDP	=	Power Delay Profile
ICI	=	Inter-Carrier Interference
ISI	=	Inter-Symbol Interference
RIO	=	Reconfigurable I/O

Chapter 1

Introduction

Massive Multiple-Input Multiple-Output (MIMO) technology has emerged as one of the most promising communication technologies in terms of bit rate, spectrum usage, and energy efficiency, and is one of the main areas of Fifth-Generation (5G) wireless research. Through this technology, next-generation wireless data networks aim at accommodating more users at higher throughput rates, all while providing higher reliability and consuming less power [7]. However, it has proven difficult to prototype and perform real-world measurements, as setting up realistic scenarios between large antenna arrays requires huge amounts of overhead and complexity. Computer simulations are possible, but require lots of simplifications, and it is difficult to tell how such simulation results compare to a real-world experiment. In recent years, however, National Instruments (NI) has developed a Massive MIMO framework that enables researchers to rapidly prototype large-scale antenna systems that can run in real-time, and transmit and receive radio frequency (RF) signals under real-world channel conditions [7]. This framework can be used for real-world scenario prototyping and has recently been acquired by the Norwegian University of Science and Technology (NTNU).

1.1 Motivation and Thesis Scope

This thesis is part of a larger project led by post-doctoral researcher Indrakshi Dey and supervised by professor Pierluigi Salvo Rossi. The aim of said project is to look at how the Massive MIMO framework described above can be used to model a specific research area called *decision fusion* (DF) in wireless sensor networks. This research area is more closely described in section 2.8.3, but in short, DF is a technique used in statistics and pattern recognition to combine classifiers to achieve a better classification accuracy [17]. In the case of wireless sensor networks, DF consists of transmitting local decisions of an observed event to a *Decision Fusion Center* (DFC) that then takes a global decision based on the decisions transmitted from each individual sensor. This DFC is to be equipped with a large antenna array, where the number of antennas far exceeds the number of transmitting sensors in the network. Testing such a system with a real-world prototype will hopefully

show that DF algorithms developed for a Massive MIMO DFC exceeds the reliability performance in comparison to the non-MIMO case.

The main emphasis of this thesis is to assist said project leader in designing the experiment setup, making necessary code configurations, and outlining the possibilities the Massive MIMO framework has to offer, as well as the challenges and limitations in regards to the considerable complexity of the framework. If time permits, an analysis of the obtained results will also be presented.

1.2 Existing work and literature

There has been quite a bit of theoretic research done around the area of decision fusion in wireless sensor networks. The procedures and algorithms that this thesis will focus on can be found in the papers "Massive MIMO Channel-Aware Decision Fusion" [16] and "Wideband Collaborative Spectrum Sensing using Massive MIMO Decision Fusion" [18], with much of the background theory explained in the paper "Channel-Aware Decision Fusion in Distributed MIMO Wireless Sensor Networks: Decode-and-Fuse vs. Decode-then-Fuse" [19].

As the NI Massive MIMO framework wasn't released until last year [20], there isn't an extensive amount of research available in regards to practical results obtained from real-world measurements, both because not many institutions have yet acquired said framework, and because those that have, haven't had enough time to conduct many experiments yet. In fact, as far as the author knows, this project is the first of its kind at NTNU. However, two of the main institutions that have acquired said framework are Lund University and the University of Bristol, and a joint research project between the two managed to achieve a 12-fold increase in spectrum efficiency by using the framework [21], which shows the early Massive MIMO potential. This is further explained in section 3.2

1.3 Thesis outline

- Chapter 2 explains the background theory for the later parts of the thesis, with emphasis on communication theory and digital communication, as well as some topics in statistics.
- Chapter 3 outlines the necessary tools and equipment for the experiment setup, almost exclusively being hardware and software from NI. Similar setups from other institutions are also described.
- Chapter 4 explains the experiment design, the system model used to generate simulation results, and how software was created and modified to obtain results.
- Chapter 5 presents and discusses the obtained results.
- Chapter 6 provides a conclusion and presents possible future work to build on the work outlined in this thesis.

Chapter 2

Theory

This chapter includes the main theory elements necessary for the experiment design in chapter 4. It is assumed that the reader is familiar with the fundamentals of signal processing and wireless communication theory.

2.1 Wireless Sensor Networks

National Instruments defines a wireless sensor network (WSN) as "wireless network consisting of spatially distributed autonomous devices using sensors to monitor physical or environmental conditions." [22]. In other words, a WSN is often deployed to monitor external physical events, such as environmental monitoring, structural health monitoring, industrial machine monitoring, process monitoring, and asset tracking. In recent times, WSNs have even been used inside the human body to monitor the health of various organs. A typical topology of a WSN might look as in 2.1:

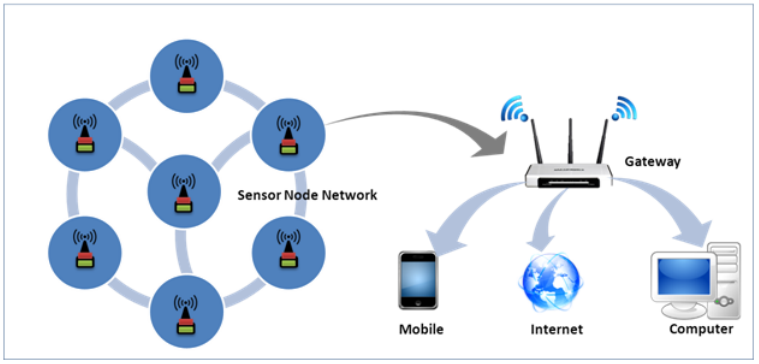

Figure 2.1: WSN topology [2]

Where the gateway usually represents a sink node such as a base station. Transmission

technologies used for communication between the sensor nodes and the gateway varies depending on the WSN topology and physical conditions, some examples being Wi-Fi, Bluetooth, Ultra Wideband, ZigBee, etc... [23]. One of the major advantages of WSNs is its resilience when it comes to sensor failures, meaning that a failure in one of the sensor nodes in the network won't compromise the entire system. Said sensors are usually small, lightweight, and mobile, and uses a battery as a power source.

2.2 Massive MIMO

2.2.1 MIMO definition and advantages

In traditional communication systems, two wireless nodes communicate by transmitting and receiving data over a radio channel, with one antenna at each end. This radio channel uses a certain amount of spectrum, and said spectrum is often scarce in certain areas where there are many different systems wanting to transmit simultaneously. Multiple Input Multiple Output (MIMO) is a range of technologies used to increase the communication capacity without requiring more spectrum. Many modern technologies, such as Wi-Fi 802.11ac and LTE (4G) uses MIMO techniques for improving spectrum capacity [24]. Figure 2.2 shows the difference between a single-input-single-output (SISO) and a 2x2 MIMO system.

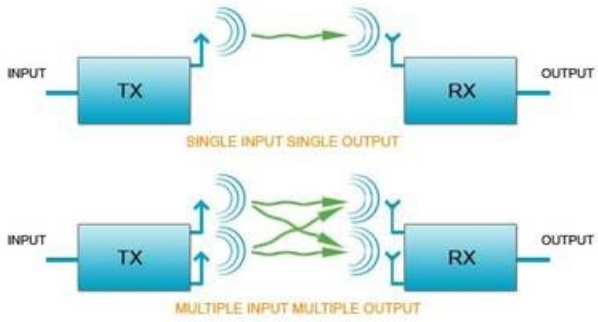

Figure 2.2: SISO vs MIMO [3]

Three of the most important features of MIMO systems are *array gain*, *diversity gain*, and *spatial multiplexing gain*. *Array gain* is simply the total improved antenna gain in comparison to the SISO case. *Diversity gain* is the technique of sending the same information over several independent fading channels. One of the major advantages is that due to the statistical properties of independently fading channels, it is unlikely that both channels will fade simultaneously. Figure 2.3, which shows the decibel signal strength from multichannel measurements done at the Chalmers University of Technology, compares how the same information sent over several channels varies in regards to channel characteristics. As can be seen, the signal has several fades in all of the channels, but rarely at the same time. Thus, diversity is often used to combat fading and provide higher transmission reliability. *Spatial multiplexing gain* is the technique of sending independent information

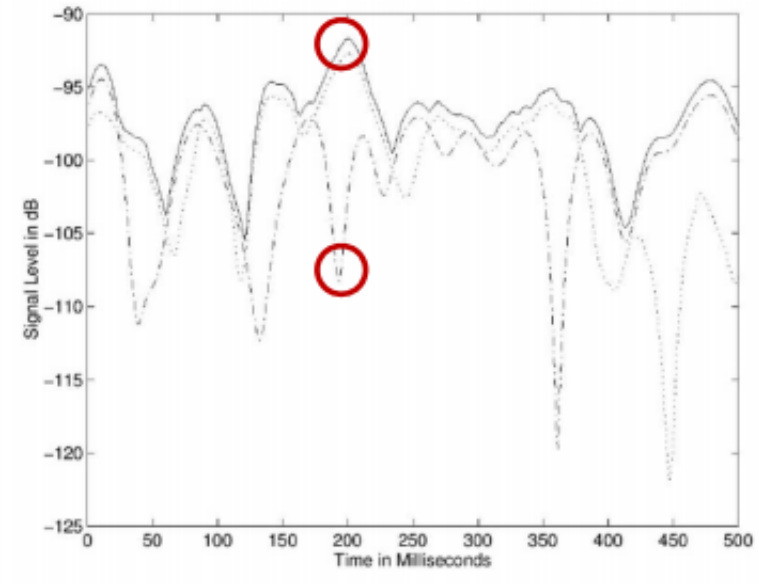

Figure 2.3: Diversity gain illustration [4]

over each spatial channel. For example, if one is sending three information bits over a communication channel with three available antennas, one would send one bit on each antenna. The most obvious advantage of this is higher throughput, as one can send three bits per time unit by using all available antennas, instead of just one in the single antenna case. Figure 2.4 illustrates the difference between diversity and spatial multiplexing.

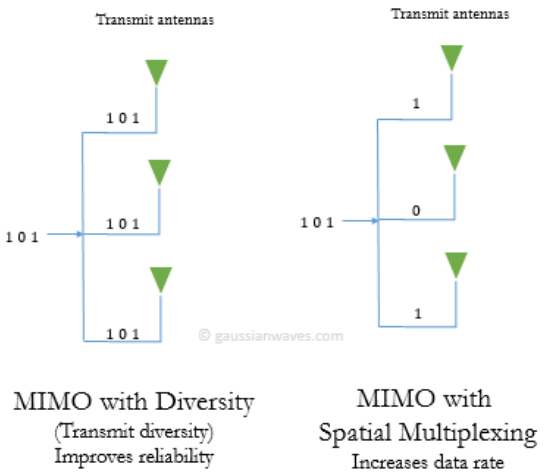

Figure 2.4: Diversity gain illustration [5]

2.2.2 Massive MIMO description

Massive MIMO in modern communication standards usually refers to systems where the number of antennas at the base station far exceeds the number of user equipment (UE) connected to said base station. Figure 2.5 shows an example of the massive MIMO concept.

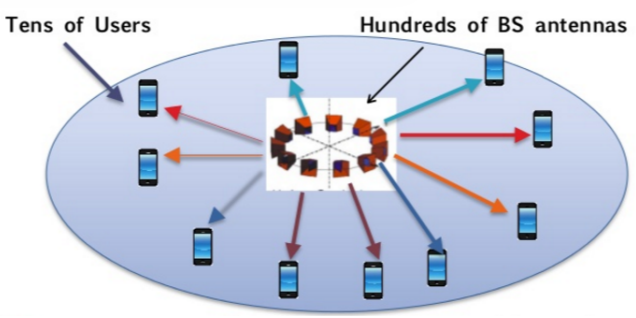

Figure 2.5: Massive MIMO illustration [6]

The main advantages of Massive MIMO, much in part due to the features described in section 2.2.1, are major improvement in spectral efficiency, reliability, and energy efficiency [6]. Figure 2.6 shows a comparison between IMT-advanced and IMT-2020 standards, also commonly known as 4G and 5G respectively, where Massive MIMO is expected to play a central part in the latter.

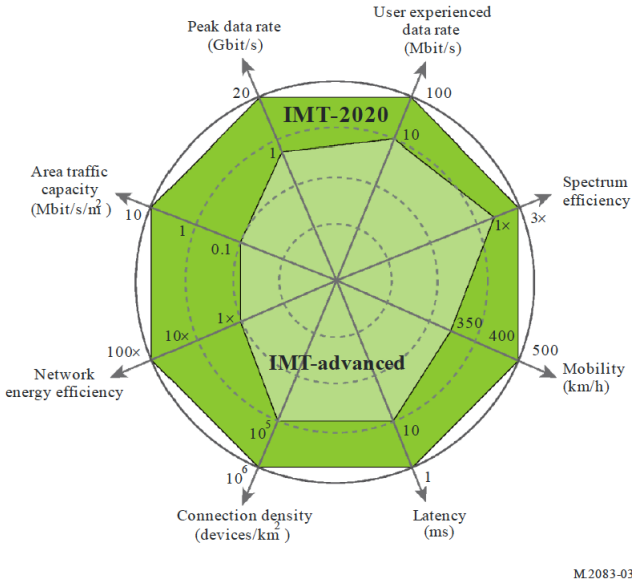

Figure 2.6: Massive MIMO illustration [7]

2.3 Digital Communication and Signal Processing

2.3.1 Binary Phase Shift Keying (BPSK)

Phase shift keying (PSK) is a digital modulation scheme where the phase of a signal is used to represent different information symbols. The simplest PSK technique is called Binary Phase Shift Keying (BPSK), where only two different symbols are used to transmit one bit at a time. The pair of signals $s_1(t)$ and $s_2(t)$, used to represent symbols 1 and 0 respectively, are defined by:

$$s_1(t) = \sqrt{\frac{2E_b}{T_b}} cos(2\pi f_c t) \qquad 0 \leq t \leq T_b \tag{2.1}$$

and

$$\begin{aligned} s_2(t) &= \sqrt{\frac{2E_b}{T_b}} cos(2\pi f_c t + \pi) \\ &= -\sqrt{\frac{2E_b}{T_b}} cos(2\pi f_c t) \qquad 0 \leq t \leq T_b \end{aligned} \tag{2.2}$$

Where T_b is the bit duration period, E_b is the transmitted signal energy per bit, and f_c is the transmission carrier frequency. As can be seen from equation 2.1 and 2.2, each of the signals are 180 degrees out of phase with each other. Figure 2.7 shows a binary stream and the corresponding modulated BPSK waveform.

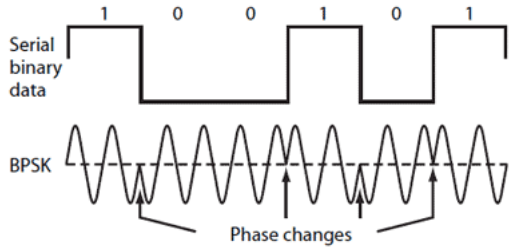

Figure 2.7: Binary stream and corresponding waveform [8]

2.3.2 Orthogonal Frequency Division Multiplexing (OFDM)

In regular Frequency Division Multiplexing, a given bandwidth is divided among a set of carriers. OFDM is a special case of FDM where closely spaced orthogonal sub-carrier signals are used to carry and transmit data on several parallel channels. Each sub-carrier is modulated with some digital modulation scheme carrying low-rate data streams, where the total rate across all sub-carriers is similar to what it would be in the single-carrier scenario with the same total bandwidth. The main difference between FDM and OFDM is how the subcarriers in OFDM are carefully designed to be orthogonal to each other, eliminating

the need for guard bands between sub-channels. This orthogonality is achieved through designing the peaks of each individual subcarrier to be located exactly at the zero-crossings of all the other subcarriers. An illustration of this, as well as an illustration of the difference between FDM and OFDM can be seen in figure 2.8 and 2.9, respectively.

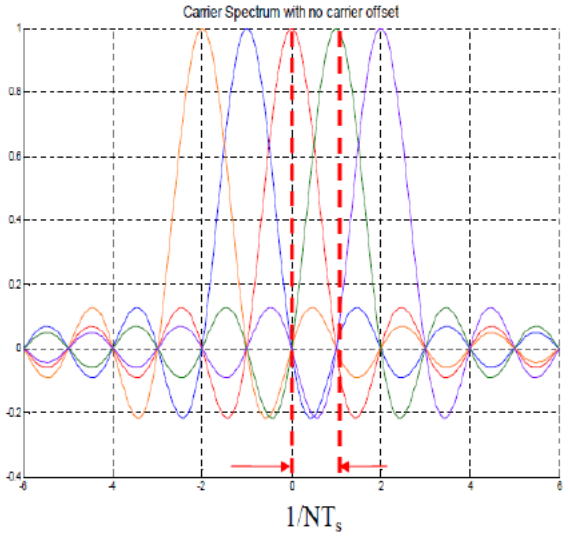

Figure 2.8: OFDM Orthogonality illustration (T_s is the useful symbol period) [9]

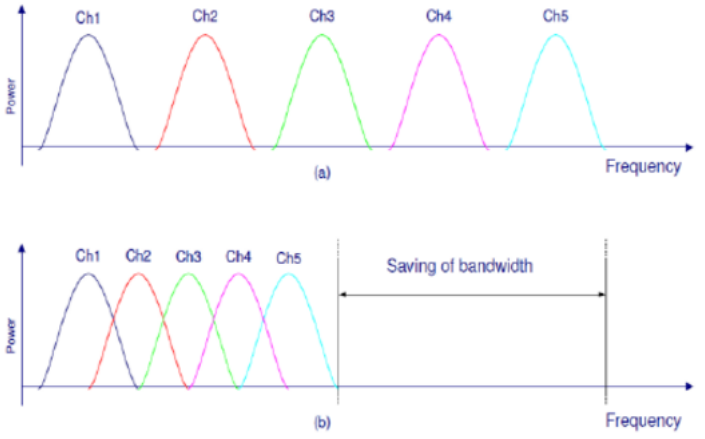

Figure 2.9: FDM vs OFDM illustration [9]

The advantages of OFDM as many of the same as in FDM, namely:

- Many signals can be transmitted simultaneously.

- Easier demodulation due to slower data rates.
- High resistance to non-ideal channel conditions such as attenuation and narrowband fading as it only affects single channels instead of the entire used spectrum [25].

However, one of the main advantages of OFDM specifically, as can be clearly seen in figure 2.9 is the improvement in spectral efficiency it offers due to less bandwidth being needed for the same amount of carriers with the same data rate.

The approach of designing an OFDM communication system is quite complex, and large parts of digital communication courses are often dedicated to covering this, so this section won't go into much detail on how to do this. However, an overall block diagram is shown in figure 2.10.

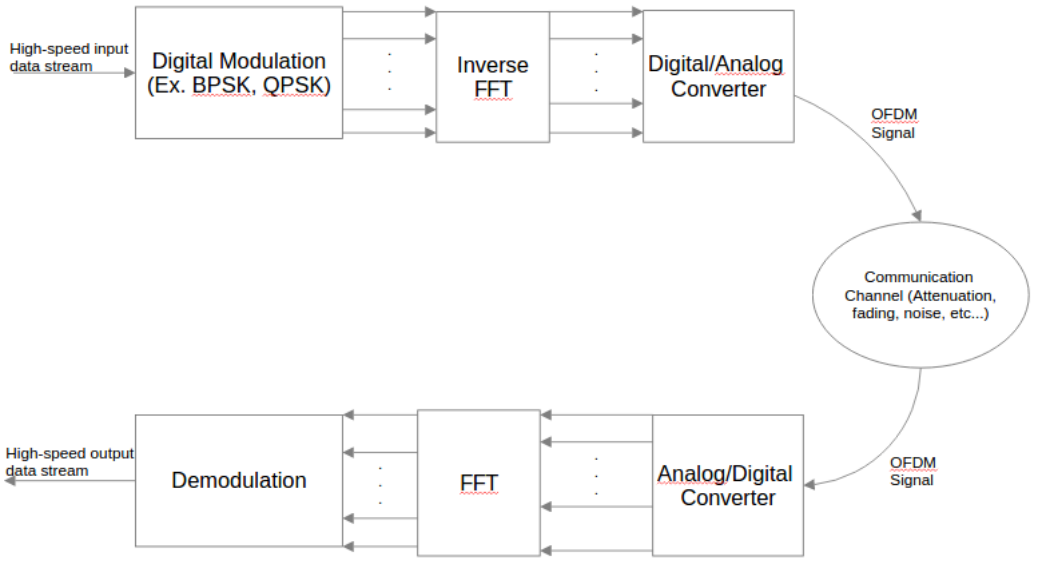

Figure 2.10: OFDM Communication System

2.4 Cognitive Spectrum Sensing

Cognitive radio (CR) is a wireless communication technology where the transceiver intelligently detects which communication channels are in use. The motivation for employing such a technology is to better utilize available RF spectrum. There are two main types of CR: *Full Cognitive Radio*, in which all parameters observable by a node in a wireless network is considered, and *Spectrum-Sensing Cognitive Radio*, where only the RF spectrum is considered. The latter is the most relevant for this thesis.

In spectrum-sensing cognitive radio, a typical scenario is where there is a primary user (PU), and several secondary users (SU), sometimes referred to as cognitive users or cognitive radios (CR). The secondary users are allowed to use a certain spectrum space as long as it is not in use by the PU. Therefore, the SUs must continuously sense the spectrum. Unused spectrum will typically show white noise characteristics. In certain cognitive spectrum sensing methods, such as centralized cooperative spectrum sensing, decisions from each SU about whether the spectrum is in use by a PU is sent to a fusion center that takes a final decision about whether there is a signal present from the primary user. Figure 2.11 shows an illustration of centralized cooperative spectrum sensing.

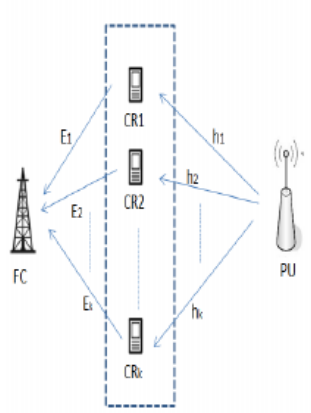

Figure 2.11: Centralized cooperative spectrum sensing illustration [10]

The concept of decision fusion is further explained in section 2.8.3

2.5 Wireless channel characteristics

A wireless radio communication channel generally refers to the physical transmission medium in a telecommunication network. The transmission properties thus heavily depend on the physical characteristics of the environment where the radio signals are transmitted. Three of the main components that influence radio propagation models are:

1. *Path loss*: Signal attenuation due to transmission over a certain distance.
2. *Shadowing*: Signal attenuation due to penetration of large objects, such as buildings and walls.
3. *Fading*: Signal alteration due to multipath transmissions, often due to reflections causing multiple radio paths.

Channel models are often created as a combination of statistical and physical factors, with variables such as fading and noise following some statistical distribution, and path

loss being modeled as a function of the distance between the antennas and the wavelength of the transmitted signal.

2.5.1 Indoor propagation

Indoor propagation behaviour differs from other traditional models in that transmission distances are much smaller, and the environment variation differs greatly. There are usually a lot more reflectors in the environment, such as walls, tables, etc... which causes a lot more multipath signal components to arrive at a much lower delay spread. Also, the behaviour is strongly influenced by building layout and the material of said reflectors. This has a great effect on the strength of transmitted signals, and needs to be accounted for in situations such as selecting a PU signal presence threshold for the cognitive sensing scenario described in section 2.4.

2.5.2 Favorable Propagation

Favorable propagation is defined as mutual orthogonality among vector-valued channels. In mathematical terms, given channel vectors $\{\mathbf{g}_k\}, k = 1, ..., K$, a channel offers favorable propagation if:

$$\mathbf{g}_i^{\mathsf{H}}\mathbf{g}_j = \begin{cases} 0, & i, j = 1, ..., K, \quad i \neq j \\ ||\mathbf{g}_k||^2, & k = 1, ..., K, \quad i = j \end{cases} \tag{2.3}$$

This is one of the main radio channel properties exploited in Massive MIMO, as it offers the most desirable scenario for maximizing the system capacity. For instance, one can use linear processing techniques, such as matched filtering at the receiver, to cancel out noise and interference [26].

In practice, equation 2.3 will never be exactly satisfied, only approximately. A common assumption is that a MIMO channel offers *asymptotically favorable* propagation, that is:

$$\lim_{M \to \infty} \frac{1}{M} \mathbf{g}_i^{\mathsf{H}}\mathbf{g}_j \to 0 \tag{2.4}$$

Where M is the number of antennas at the base station.
The above assumptions can be used to derive optimal capacity results, which can be seen in the proceedings paper Aspects Of Favorable Propagation in Massive MIMO [26].

2.5.3 Power Delay Profile (PDP)

The PDP shows the distribution of the power of a received signal over a multipath channel as a function of the delay of the signal propagation. It is often denoted as $p(\tau)$, and is obtained as the spatial average channel impulse response, written as:

$$p(\tau) = E[|h(t, \tau|^2] \tag{2.5}$$

A PDP plot is usually illustrated as the signal power at the receiver as a function of the propagation delays.

Delay Spread

The delay spread measures the multipath richness of a communication channel, and can be derived from the PDP. As multiple components of the same signal arrives at the receiver at different times, one can view the delay spread as the difference in time between the first and last arriving signal component of significant energy. Its computation is similar to the standard deviation of a statistical distribution, and for a discrete channel it is calculated as:

$$\bar{\tau} = \frac{\sum \tau p(\tau)}{\sum p(\tau)} \tag{2.6}$$

For continuous channels, replace the summations with integrals and integrate with respect to $d\tau$.

2.5.4 Channel Reciprocity

Channel reciprocity is the condition that in a wireless communication system with a transmitter and a receiver, both transmission links match exactly. Thus, if the channel reciprocity condition holds, the uplink channel estimation can also be used to characterize the downlink channel.

2.6 Maximum Ratio Combining (MRC)

Maximum ratio combining is a receiver technique used in communication systems with multiple receiver antennas. It aims at restoring the original transmitted signal by:

1. Adding signals from each of the channels together.
2. Adjusting the gain of each channel to be proportional to the RMS signal level and inverse proportional to the mean square noise level of said channel.
3. Using different proportionality constants for each channel.

2.6.1 Mathematical description

Consider a system with one transmit antenna and N receive antennas. Let the received signal on the i'th antenna be:

$$y_i = h_i x + n_i \tag{2.7}$$

where

- y_i is the received signal
- h_i is the channel coefficient on the i'th receive antenna
- x is the transmitted symbol
- n_i is the noise on the i'th antenna

Expressing the entire received signal in vector for becomes:

$$\mathbf{y} = \mathbf{h}x + \mathbf{n} \tag{2.8}$$

Where

$$\mathbf{y} = [y_1\ y_2\ ...\ y_N]^{\mathsf{H}} \tag{2.9}$$

$$\mathbf{h} = [h_1\ h_2\ ...\ h_N]^{\mathsf{H}} \tag{2.10}$$

$$\mathbf{n} = [n_1\ n_2\ ...\ n_N]^{\mathsf{H}} \tag{2.11}$$

Where H denotes the Hermitian transpose. The equalized symbol, $\hat{x}$, becomes

$$\begin{aligned} \hat{x} &= \frac{\mathbf{h}^{\mathsf{H}}\mathbf{y}}{\mathbf{h}^{\mathsf{H}}\mathbf{h}} \\ &= \frac{\cancel{\mathbf{h}^{\mathsf{H}}\mathbf{h}}x}{\cancel{\mathbf{h}^{\mathsf{H}}\mathbf{h}}} + \frac{\mathbf{h}^{\mathsf{H}}\mathbf{n}}{\mathbf{h}^{\mathsf{H}}\mathbf{h}} \\ &= x + \frac{\mathbf{h}^{\mathsf{H}}\mathbf{n}}{\mathbf{h}^{\mathsf{H}}\mathbf{h}} \end{aligned} \tag{2.12}$$

Let

$$n' = \frac{\mathbf{h}^{\mathsf{H}}\mathbf{n}}{\mathbf{h}^{\mathsf{H}}\mathbf{h}} \tag{2.13}$$

Equation 2.12 thus simplifies to

$$\hat{x} = x + n' \tag{2.14}$$

As can be seen, through the use of MRC, the estimate of the originally transmitted symbol, $\hat{x}$, simplifies to the originally transmitted symbol plus noise, and attenuation caused by the channel coefficients are negated. The above derivation is for the case where there is only one transmit antenna (though several receive antennas). With several transmit antennas, the expressions get more complex, but the thought process remains the same. An illustration of a 1x2 single-input multiple-output (SIMO) system can be seen in figure 2.12.

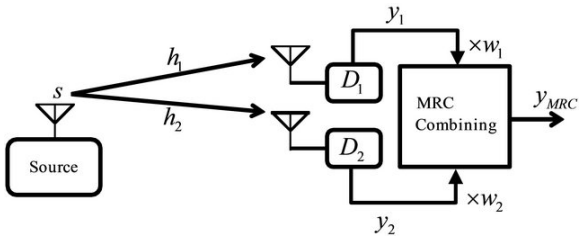

Figure 2.12: 1x2 antenna MRC system [11]

As might be obvious, implementing such scheme requires full channel state information (CSI) knowledge at the receiver.

2.7 Software Defined Radio (SDR)

An SDR is a radio communication system where components that have traditionally been implemented in hardware, such as filters, modulators, and amplifiers, are instead implemented as software. For example, a capacitor and a diode in a demodulator would be replaced by a digital signal processing script implemented on a digital platform such as an embedded system. The SDR concept is not new, but has become increasingly available in recent years due to the rapid advance in the sophistication of digital electronics and digital signal processing algorithms. Figure 2.13 shows an example of a typical block diagram for an SDR:

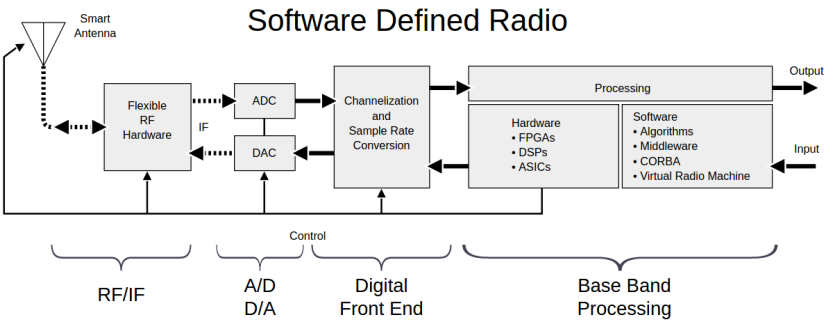

Figure 2.13: SDR block diagram example [12]

2.7.1 Advantages

The main advantage of an SDR compared to a traditional radio communication system lies in its flexibility in that radio protocol specifications can be changed in real-time. This is especially useful in scenarios where one needs to dynamically change frequency specifications, such as in cognitive radio techniques. In traditional systems, this would require expensive and complex hardware, but becomes much cheaper and easier with proper SDR equipment. SDR products are also considered to be more stable, as results produced by hardware components are subject to factors such as age and temperature variations, whereas software will always produce the same results. Thus, results are easier to predict and reproduce with an SDR.

2.8 Statistics

2.8.1 Hypothesis testing

A hypothesis test is a test based on statistics that determines whether there is enough evidence in a data set to infer whether one can make a certain conclusion about an entire population. The test consists of two opposing hypotheses: the null hypothesis and the alternative hypothesis, often referred to as $\mathbf{H_0}$ and $\mathbf{H_1}$. $\mathbf{H_0}$ represents the "no difference" or the "status quo" hypothesis, and $\mathbf{H_1}$ represents the condition that is being tested. A

hypothesis test is not designed to select the most likely of $\mathbf{H_0}$ and $\mathbf{H_1}$. Instead, it will remain with $\mathbf{H_0}$ until there is enough evidence to conclude the validity of the alternative hypothesis $\mathbf{H_1}$. A hypothesis test always arrives at one of the following two conclusions:

- *Reject* $\mathbf{H_0}$ in favor of $\mathbf{H_1}$ because of sufficient evidence in data
- *Fail to reject* $\mathbf{H_0}$ because of insufficient evidence in data

Figure 2.14 shows the possible situations for testing a statistical hypothesis.

	H_0 **is true**	H_0 **is false**
Do not reject H_0	Correct decision	Type II error
Reject H_0	Type I error	Correct decision

Figure 2.14: Possible hypothesis testing outcomes [13]

Hypothesis testing is one of the main tools used when creating receiver operating characteristic plots, which is discussed in 2.8.4.

2.8.2 Likelihood-Ratio test

A likelihood-ratio test is a method in statistics used for comparing the goodness of fit between two statistical models. It is often used in hypothesis testing to decide whether to keep or reject the null hypothesis. The test is based on how many more times more likely the data is under one model than the other. This value is then compared to a threshold value to decide whether to keep or reject the null model. Assuming a probability density function $f(x|\theta)$, the likelihood ratio, Λ, based on the data, x, can be written as:

$$\Lambda(x) = \frac{L(\theta_0|x)}{L(\theta_1|x)} = \frac{P(x|\theta_0)}{P(x|\theta_1)} \tag{2.15}$$

Where $\theta = \theta_0$ represents the null hypothesis, H_0, and $\theta = \theta_1$ represents the alternative hypothesis, H_1. The obtained value is then compared to a treshold value, γ, based on the following rules:

- If $\Lambda > \gamma$, keep H_0
- If $\Lambda < \gamma$, reject H_0
- If $\Lambda = \gamma$, reject H_0 with some pre-defined probability

Because of the way likelihood functions are calculated, the result can become very small, which is problematic for systems with limited floating-point precision support. Therefore, the Log-Likelihood Ratio, or LLR, is often used instead, which is simply the logarithm of the likelihood function. The LLR thus becomes

$$LLR = \ln \Lambda(x) = \ln \left[\frac{P(x|\theta_0)}{P(x|\theta_1)} \right] \tag{2.16}$$

This method is often used in Decision Fusion, which will be explained in the next subsection.

2.8.3 Decision fusion

Decision fusion is a subcategory of data fusion, which is the process of integrating data from multiple sources into one consistent, accurate representation through using methods from statistics and machine learning. Decision fusion differs from data fusion in that a binary event is inferred from the data sources, such as the presence or non-presence of a certain physical events. This operation usually consists of multiple sources sending information to a DFC that combines said information and takes a binary decision. Figure 2.15 shows an example of how this with a set of sensors monitoring an external event:

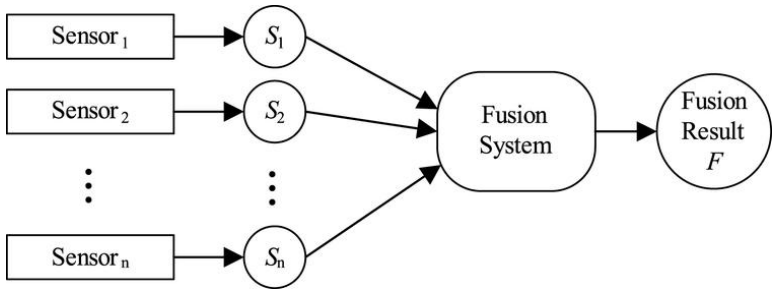

Figure 2.15: DF illustration [14]

with S_1, ..., S_n being the decision taken by each individual sensors, and F being the binary decision from the algorithm implemented in the DFC.

2.8.4 Receiver Operating Characteristics (ROC)

A ROC curve is a graphical plot that shows how a binary classifiers performance varies as one changes its discrimination threshold. This performance curve is illustrated by plotting the *true positive rate* (TPR), also called the *sensitivity* or *probability of detection*, on the vertical axis against the *false positive rate* (FPR), also called the *fallout* or *probability of false alarm* on the horizontal axis at various threshold values. The ROC curve thus represents the TPR as a function of the FPR. Figure 2.16 shows an illustration of the ROC space, and figure 2.17, with the red curve illustrating what a non-random ROC curve for a classifier might look like.

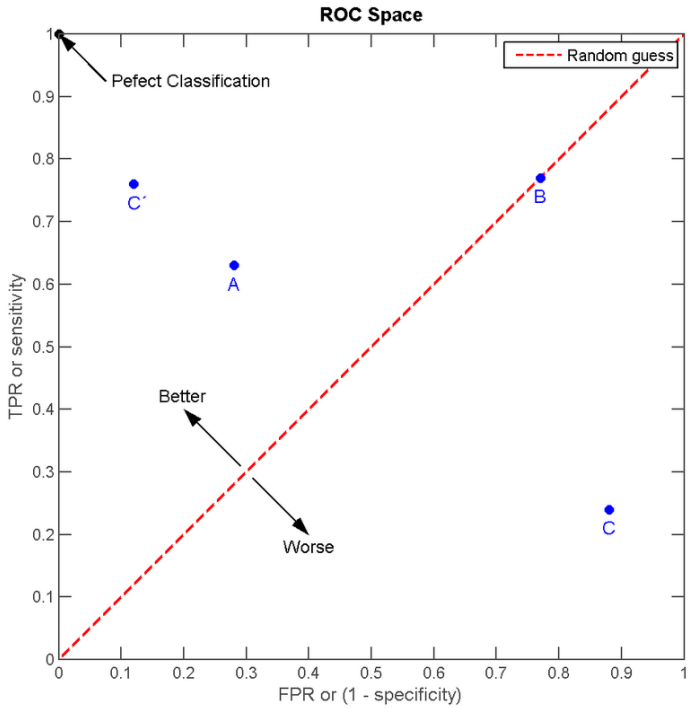

Figure 2.16: ROC illustration

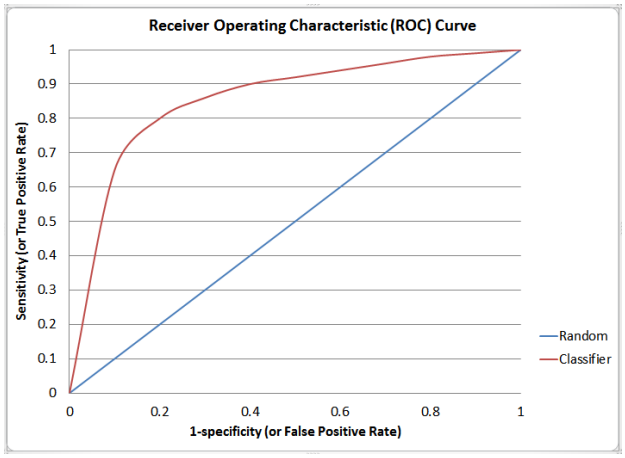

Figure 2.17: ROC curve example

Chapter 3

Relevant Tools and Similar Setups

3.1 Software and Hardware

3.1.1 NI-USRP Software Defined Radio

Universal Software Radio Peripheral (USRP) is a range of software defined radios developed by National Instruments (NI), and is a commonly used SDR hardware platform used by research labs and universities. Their main use is to enable prototyping of wireless communications systems through programming languages such as gnuradio or LabVIEW. Figure 3.1 shows an image of an NI USRP-2901 SDR from the radio communications lab at NTNU.

This particular USRP device offers frequency ranges from 70 MHz up to 6 GHz, and the hardware supports four antenna ports: two for transmitting and two for receiving. The device also has input ports for synchronization signals, timing signals, and external power connectors.

3.1.2 LabVIEW Communications Design Suite

Laboratory Virtual Instrument Engineering Workbench, or LabVIEW, is a visual programming design platform from NI. The programming language used is called G, which is a visual data flow language. Some of its main purposes are data acquisition, instrument control, and signal processing. LabVIEW program flow is determined by the connection of graphical block diagrams through the use of wires. These wires propagate variables, and block nodes execute as soon as all input data is available. Said block nodes generally consists of inputs, also called controls, and outputs, also called indicators. Multithreading is supported by the scheduler, and thus several variables can propagate through different wires at the same time.

The LabVIEW Communications Suite is a specific LabVIEW design environment created for rapidly prototyping communications systems. Figure 3.2 shows an example of an OFDM modulator program written in the LabVIEW Communications Design Suite.

Figure 3.1: NI USRP-2901 software-defined radio

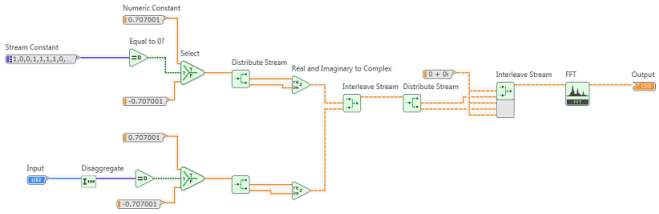

Figure 3.2: LabVIEW OFDM modulator example

There are several advantages of using the LabVIEW Communications Design Suite. Firstly, it contains a wide range of optimized block nodes for communications and signal processing algorithms. Secondly, the platform is designed for easy interfacing with hardware communication platforms such as NI USRP SDRs. Other advantages include an active user community and the ease and speed of code compilation.

3.1.3 NI MIMO Application Framework at NTNU

The NI MIMO Application Framework is designed to provide a hardware and software combination for MIMO prototyping and testing. With said framework, researchers can create Massive MIMO testbeds to rapidly prototype large-scale antenna systems and evaluate how real-world results compare to theoretical simulations. The system is designed with the LabVIEW Communications System Design Suite 2.0 running on USRP SDR hardware, allowing system scaling from a 4-antenna up to a 128-antenna system.

The framework is mainly built up of two parts: the Base Station (BS) host, and the Mobile Station (MS) host, where the MS acts as a mobile unit. Both uplink and downlink configurations are provided, and the framework has a modular design approach such that developers can focus on specific parts of the system that they wish to modify. It also provides a panel for easy transmitter and receiver configuration specifications such as bandwidth, RF frequency, detection algorithms, transmit power, receiver gain, modulation type, and much more. Specific details can be found in the MIMO Application Framework white paper [27]. A typical system model of how a Massive MIMO BS communicates with user equipment can be seen in figure 3.3.

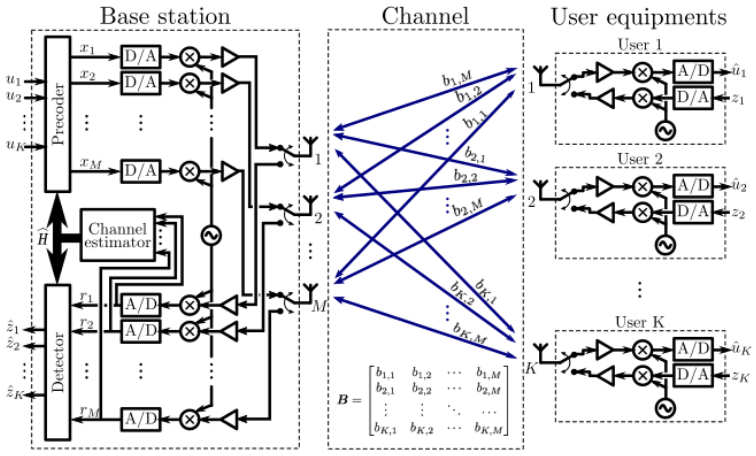

Figure 3.3: Generic Massive MIMO System Model [15]

At NTNU, the current setup as of late spring 2017 is a 64-antenna rack, with a plan to expand to eventually expand to 128 antennas. The setup can be viewed in figure 3.4.

As can be seen from the figure, the setup is equipped with 32 USRP Reconfigurable I/O (RIO) devices, each equipped with two rubber-duck antennas. The testbed is also

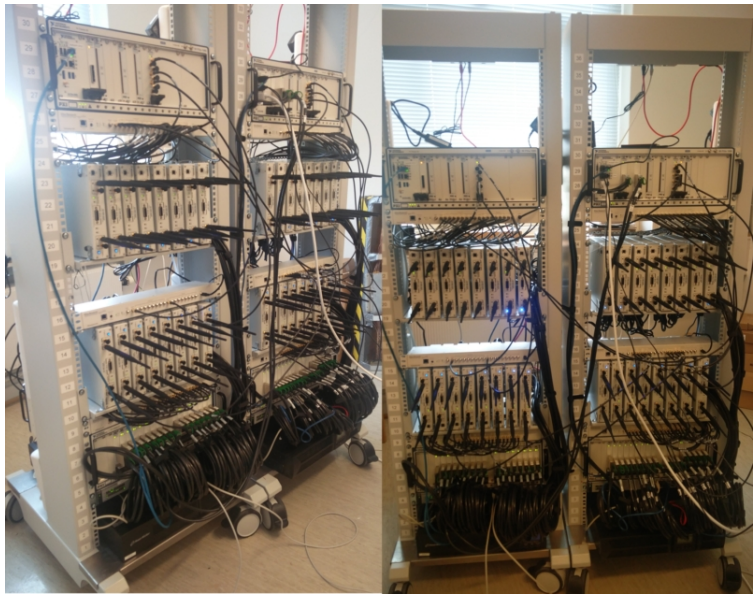

Figure 3.4: NTNU 64-antenna Massive MIMO setup

configured to communicate with a certain amount of UEs, but this will be further explained in the experiment setup in section 4.5

3.2 Similar Setups

Other than NTNU, Lund University and the University of Bristol are two of the main institutions experimenting with similar setups. This section will briefly describe the testbed configurations and obtained results from said institutions.

3.2.1 Lund University

The details of the most recent description of the Massive MIMO setup at University of Lund can be viewed in [15]. Like at NTNU, this system consists mainly of hardware from NI.

The Lund Massive MIMO testbed, abbreviated as LuMaMi, claims to be the first reconfigurable real-time hardware platform for ptototyping massive MIMO. This setup consists of 100 antennas by using 50 SDRs at the base station, and serving up to 12 UEs through an LTE-like OFDM scheme. This system has been tested both indoors and outdoors, with various precoding and decoding schemes. The field results, which were obtained in a measurement campaign in 2016, showed that it is possible to separate as many as 12 UEs using the same time and frequency resources in a Massive MIMO setup. Figure 3.5 shows the

LuMaMi testbed which includes an in-house developed T-shaped antenna array in order to improve isolation and bandwidth efficiency.

Figure 3.5: LuMaMi testbed at Lund University [15]

3.2.2 University of Bristol

Detailed description of the Massive MIMO setup and overview of the ongoing related research at the University of Bristol (UoB) can be viewed in [1].

The Massive MIMO testbed at UoB consists of a 64-SDR, 128-antenna real-time testbed, and was developed in collaboration with NI and Lund University. Through trials performed in 2016, an experiment with UEs placed in line-of-sight, non-static environments, a throughput of approximately 3 Gigabytes per second and a spectral efficiency of 145.6 bits/s/Hz was achieved. Figure 3.6 shows the 128-antenna testbed at UoB.

Ongoing and future Massive MIMO related research at UoB includes, but is not limited to, real-time downlink performance evaluation, optimal power control, and over-the-air synchronization optimization.

Figure 3.6: Massive MIMO 128-antenna testbed at UoB [1]

Chapter 4

Envisioned Experiment Design and Implementation

This chapter aims at explaining the experiment planning. It is based on the theory and tools explained in chapter 2 and 3, and it is therefore necessary to have read these chapters before proceeding.

This chapter is divided into five sections: first, the overall envisioned system architecture is described in 4.1. Then, the hardware and software requirements are described in section 4.2. The theoretical system model and DF algorithms used for creating simulation results are explained and derived in section 4.3. The practical implementation details and encountered issues are explained in section 4.4. Finally, the applied experiment setup is explained in section 4.5.

4.1 System Architecture and Application Scenario

The setup can be modeled as a cognitive machine-to-machine type of communication scenario where a set of mobile units communicate with a DFC through a centralized cooperative sensing approach as shown in figure 2.11. The system consists of one PU, K SUs, and one DFC with N antennas, where $N >> K$. The entire spectrum is divided into L sub-channels. Each of the SUs will sense these L frequency bands and transmit a 1-bit symbol to represent whether the PU is active or not, with 0 being inactive and 1 being active. The DFC will then apply a DF algorithm on the data provided by the SUs to take a final decision on whether the spectrum is in use by the PU. Both the PU and the SUs are equipped with one transmit antenna. The setup is illustrated in figure 4.1

One can generally consider a frequency band as unoccupied if it consists only of noise. In the opposite case the frequency band will consist of a signal-noise combination. This can be modeled as a binary signal detection problem, which again can be modeled as a hypothesis testing problem. The role of the DFC is to provide a reliable decision about signal presence based on the transmitted decision of each of the independent SUs. The

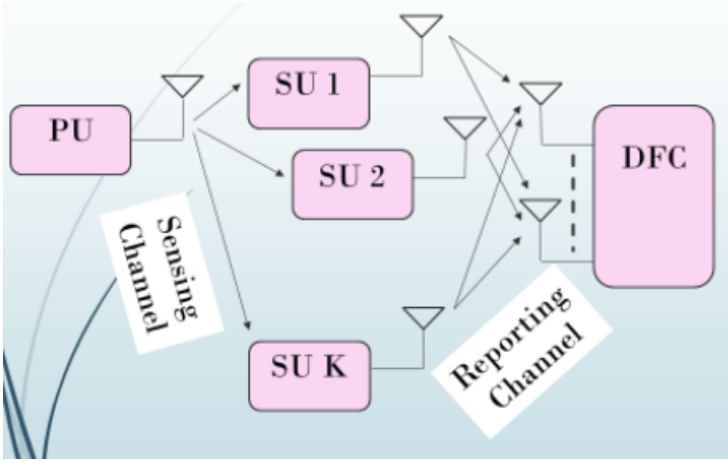

Figure 4.1: Application scenario

multi-antenna setup of the DFC means the system can be labeled as a virtual massive MIMO channel, and is thus able to exploit diversity and combat fading and shadowing issues.

4.2 Requirements

4.2.1 Hardware Requirements

The hardware requirements can be divided into two parts: the requirements for the transmitter side, and requirements for the receiver side. For the transmit side, the following is needed:

- One SDR to act as the PU, intermittently sending on each of the frequency bands.
- Six SDRs to act as the SUs, each continuously sensing each of the spectrum frequency bands and transmitting decisions regarding used spectrum.
- Two computers, one for controlling the PU and one for controlling the SUs.

As for the receiver side:

- A massive MIMO rack as described in 3.1.3, equipped with 64 antennas. This will act as the DFC.
- One host computer for controlling the DFC and performing post processing DF algorithms.

The envisioned hardware setup is illustrated in figure 4.2.

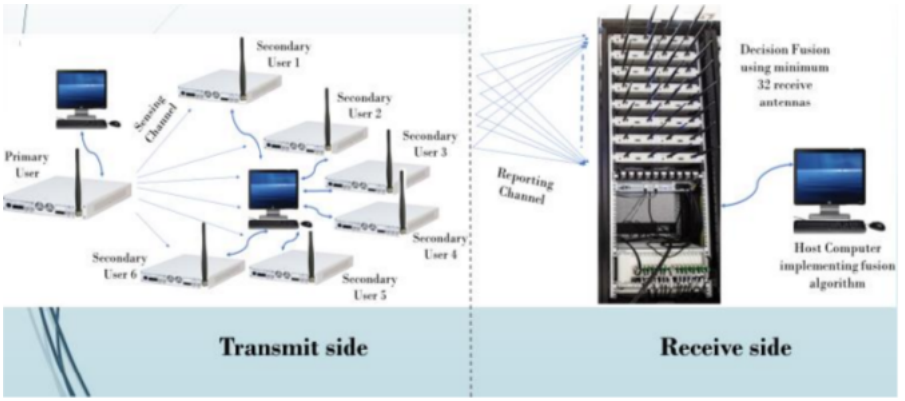

Figure 4.2: Envisioned Hardware Setup

4.2.2 Software Requirements

Again, the requirements can be divided into the transmit and receiver side. As for the transmit side, the following is needed:

- Implement a program on the PU to intermittently transmit random bit sequences intermittently on each frequency band.
- Implement a sensing-and-transmit program to run on each SU.
- Synchronize the SUs to sense and transmit their decisions of PU activity at the same time.

On the receive side:

- A program to receive the decisions transmitted by the SUs.
- DF algorithms on the host computer (The original idea was to implement this directly on the framework, but after consulting with NI representatives, this was concluded to be too challenging a task for a master thesis).

4.3 Theoretical System Model and DF Rules

The following description is based on section IIA from the research articles Massive MIMO Channel Aware Decision Fusion [16] and the unpublished paper Wideband Collaborative Spectrum Sensing using Massive MIMO Decision Fusion [18].

4.3.1 WSN and Sensing Model

Consider a decentralized binary hypothesis test, where K sensors are used to discriminate between $\mathcal{H} \triangleq \{H_0, H_1\}$, where $\mathcal{H}$ represents the absence or presence of a transmitted signal. Let:

- k represent the kth sensor, where $k \in \mathcal{K} \triangleq 1, 2, ..., K$
- $b_k \in \mathcal{H}$ represent the binary local decision of sensor k
- $x_k \in \mathcal{X} \triangleq \{-1, +1\}$ be the decisions that b_k is mapped to, using BPSK modulation.

The quality of the decisions for the kth sensor is characterized by the conditional probabilities for detection and false alarm, respectively

$$P_{D,k} \triangleq P(x_k = 1|H_1) \tag{4.1}$$

and

$$P_{F,k} \triangleq P(x_k = 1|H_0) \tag{4.2}$$

The sensors communicate with a DFC with N receive antennas over a wireless Multiple Access Channel (MAC), where $N >> K$, that is, the number of receive antennas exceeds the number of sensors. The overall DF model can be viewed in figure 4.3.

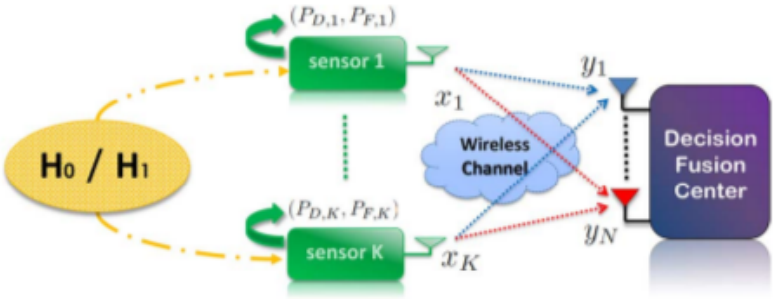

Figure 4.3: DF MIMO setup [16]

Now, consider the model as an OFDM system, where the spectrum is divided into L sub-bands. Each SU senses each of the sub-bands, and transmits their decisions on L different sub-carriers of the OFDM system.

4.3.2 Signal Model

Let the received signals at the DFC antennas be modeled as:

$$\mathbf{y}^l = \sqrt{\rho^l}\mathbf{G}^l\mathbf{x}^l + \mathbf{w}^l + \Xi^l \tag{4.3}$$

Where:

- $\mathbf{x}_k = (x_k^0, ..., x_k^{L-1})$ is the transmitted data vector from the kth SU on L sub-carriers and $\mathbf{x}^l = (x_1^l, x_2^l, ..., x_K^l)$, where $x_k^l \in \mathcal{X}$ is the BPSK symbol transmitted by the kth SU on the lth sub-carrier.
- ρ^l is the energy constraint to control the energy from each reporting sensor

- $\mathbf{y}^l \in \mathbb{C}^{N\times 1}$ is the received complex signal vector where $\mathbf{y}^l = (y_1^l, y_2^l, ..., y_N^l)$ and y_n^l is the signal received by the nth receive antenna on the lth sub-carrier.
- $\mathbf{G}^l \in \mathbb{C}^{N\times K}$ is the channel matrix that includes all the channel impulse response samples between the users and the DFC on the lth sub-carrier.
- $\mathbf{w}^l$ is the noise vector with distribution $\mathbf{w} \sim \mathcal{N}_{\mathbb{C}}(\mathbf{0}_N, \sigma_{w,l}^2\mathbf{I}_N)$
- Ξ is the interfering signal vector with distribution $\mathbf{\Xi} \sim \mathcal{N}_{\mathbb{C}}(\mathbf{0}_N, \xi_l^2\mathbf{I}_N)$

This model assumes perfect synchronization, both in time and frequency.

4.3.3 Channel Model

This subsection breaks down the channel matrix, $\mathbf{G}^l$, into several parts in order to properly model factors such as attenuation, fading, and propagation properties. This is necessary in order to generate as realistic simulations as possible to be compared to real measurements.

the channel coefficient vector $\mathbf{g}_{n,k}^l$ can be expressed as:

$$\mathbf{g}_{n,k}^l = \sqrt{\lambda_k}\mathbf{h}_{n,k}^l \tag{4.4}$$

Where λ_k models geometric attenuation and shadow-fading. $\mathbf{h}_{n,k}^l$ are the carrier interference ratios, which can be modeled as a linear time-invariant FIR filter of order Z, distributed as

$$\mathbf{h}_{n,k}^l \sim \mathcal{N}_{\mathbb{C}}(0, \text{diag}(\boldsymbol{\beta}_k^l)) \tag{4.5}$$

Where $\boldsymbol{\beta}_k^l = (\beta_k^l(0), ..., \beta_k^l(Z-1))$ is the PDP of the channel model with tap length Z. Based on the above assumptions, $\mathbf{G}^l$ can be written as:

$$\mathbf{G}^l = \mathbf{H}^l\sqrt{\mathbf{D}} \tag{4.6}$$

Where

- $\mathbf{H}^l \in \mathbb{C}^{N\times K}$ is the matrix of the fast-fading coefficients
- $\mathbf{D} \in \mathbb{C}^{K\times K}$ is a diagonal matrix where $d_{k,k} = \lambda_k$

4.3.4 Favorable Propagation Assumption

Denote the kth column of the channel matrix $\mathbf{G}^l$ as $\mathbf{g}_l^k$ being independent complex-valued Gaussians with moments

- $\mathbb{E}\{\mathbf{g}_k^l\} = \mathbf{0}_N$
- $\mathbb{E}\{\mathbf{g}_k^l(\mathbf{g}_k^l)^\dagger\} = \lambda_k * \text{diag}(\beta_k^l) * \mathbf{I}_N$

The favorable propagation conditions, assuming $N >> K$ are thus:

$$\frac{1}{N}(\mathbf{G}^l)^\dagger \mathbf{G}^l \approx \mathbf{A}^l \tag{4.7}$$

Where

$$\begin{aligned} \mathbf{A}^l &= \mathbf{D} * \text{diag}(\beta_k^l) \\ &= \text{diag}(\mathbf{\Lambda}) * \text{diag}(\boldsymbol{\beta}_k^l), \quad \mathbf{\Lambda} = (\lambda_1, ..., \lambda_K) \end{aligned} \tag{4.8}$$

4.3.5 Inter-Carrier Interference (ICI)

For a more realistic scenario, it is necessary to model of each subcarrier impact each other in terms of power. Let $\xi^2_{p,q,ICI}$ be the ICI power from subcarrier p on subcarrier q. Also, let $d_{pq} \triangleq [(q-p) \mod L]$ be the sub-carrier distance, where L is the total number of subcarriers. With the assumption that $N \to \infty$, one can approximate the ICI power between two subcarriers as:

$$\xi^2_{p,q,ICI} = \sum_K |\bar{\beta}^p_k(d_{pq})|^2 \tag{4.9}$$

Where $|\bar{\beta}^p_k(d_{pq})|^2$ is the Discrete Fourier Transform samples of the PDP between the pth and the qth subcarrier.Thus, for all L subcarrier contributing to the ICI of one subcarrier, l, the ICI can be written as:

$$\xi^2_{l,ICI} = \sum_{k=1}^{K} \sum_{p=1}^{L} |\bar{\beta}^p_k(d_{pl})|^2, \qquad p \neq l \tag{4.10}$$

4.3.6 Inter-Symbol Interference (ISI)

Again, using the assumption that $N \to \infty$, the ISI can be expressed as:

$$\xi^2_{l,ISI} = \sum_{k=1}^{K} \left| \sum_{z=0}^{Z-1} z\beta^l_k(z) \right|^2 \tag{4.11}$$

Where $\sum_{z=0}^{Z-1} z\beta^l_k(z)$ is the average delay spread of the lth subcarrier between the kth SU and the DFC. Let

$$\left| \sum_{z=0}^{Z-1} z\beta^l_k(z) \right|^2 = \bar{\tau}^2_{l,k} \tag{4.12}$$

Equation 4.11 thus becomes

$$\xi^2_{l,ISI} = \sum_{k=1}^{K} \bar{\tau}^2_{l,k} \tag{4.13}$$

4.3.7 Time-Reversed Channel Model

One of the problems with applying the channel model described above to fusion rules is the correlation between the different channels and the interference components. To combat this, one can use channel time-reversing, as this reduces the correlation while at the same time keeping desirable conditions such as favorable propagation and orthogonality between the channel matrices. Let $\check{\mathbf{G}}^l$ be the time-reversed version of $\mathbf{G}^l$. Since the channel matrices $\mathbf{G}^l$ are pairwise orthogonal, one can also assume that their time-reversed version are pairwise orthogonal as well. Like in equation 4.7, one can thus write

$$\frac{1}{N}(\check{\mathbf{G}}^l)^\dagger \check{\mathbf{G}}^l \approx \check{\mathbf{A}}^l \tag{4.14}$$

$\check{\mathbf{A}}^l$ is defined as

$$\check{\mathbf{A}}^l = \mathbf{D} * diag(\check{\boldsymbol{\beta}}_k^l) \tag{4.15}$$

Where $\check{\boldsymbol{\beta}}_k^l$ is the time-reversed version of $\boldsymbol{\beta}_k^l$ such that

$$\check{\boldsymbol{\beta}}_k^l = [\beta_k^l(Z-1), \beta_k^l(Z-2)...\beta_k^l(0)] \tag{4.16}$$

One can also make the assumption that the time-reversed version will be pairwise orthogonal to the original version, thus

$$(\check{\mathbf{G}}^l)^\dagger \mathbf{G}^l \approx \frac{1}{N}\mathbf{F}^l \tag{4.17}$$

Where

$$\mathbf{F}^l = \left(\sqrt{\mathbf{D}} * \left[diag(\sqrt{\check{\boldsymbol{\beta}}_k^l})\right]\right)^\dagger * \left(\sqrt{\mathbf{D}} * \left[diag(\sqrt{\boldsymbol{\beta}_k^l})\right]\right) \tag{4.18}$$

4.3.8 Receiver Processing

This section describes the different types of DF algorithms that are relevant for this experiment, and are based on derivations from [16] and [18]. These rules are applied in a *wideband spectrum sensing* scheme, that is, when the sensing techniques aim to sense a frequency bandwidth that exceeds the coherence bandwidth of the channel, in contrast to *narrowband spectrum sensing*, where the frequency range is sufficiently narrow such that the channel frequency response can be considered flat [28].

Optimum Rule

The *optimal test* is formulated as an LLR as follows:

$$\Lambda_{opt} \triangleq \ln\left[\frac{p(\mathbf{y}|\hat{\mathbf{H}}, \mathcal{H}_1)}{p(\mathbf{y}|\hat{\mathbf{H}}, \mathcal{H}_0)}\right] \tag{4.19}$$

Where $\mathcal{H}_0$ is kept if Λ_{opt} is less than some threshold γ, and rejected vice versa. As $\mathbf{y}$ is independent from $\mathcal{H}_i$ [16], an explicit expression of equation 4.19 can be written as

$$\Lambda_{opt}^{l} = \ln\left[\frac{\sum_{\mathbf{x}^1\in\mathcal{X}^K}\exp\left(\frac{||\mathbf{y}^l-\hat{\mathbf{G}}^l\mathbf{x}^1||^2}{\sigma_{e,l}^2}\right)P(\mathbf{x}^l|\mathcal{H}_1^l)}{\sum_{\mathbf{x}^l\in\mathcal{X}^K}\exp\left(\frac{||\mathbf{y}^l-\hat{\mathbf{G}}^l\mathbf{x}^l||^2}{\sigma_{e,l}^2}\right)P(\mathbf{x}^l|\mathcal{H}_0^l)}\right] \underset{\hat{\mathcal{H}}=\mathcal{H}_0}{\overset{\hat{\mathcal{H}}=\mathcal{H}_1}{\gtrless}} \gamma^l \tag{4.20}$$

Where $\sigma_{e,l}^2$ is the total noise and interference power densities, which can be written as:

$$\sigma_{e,l}^2 = \sigma_{w,l}^2 + \xi_l^2 \tag{4.21}$$

Where $\sigma_{w,l}^2$ is the noise power density and ξ_l^2 is the total interference power density for the given subcarrier, that is:

$$\xi_l^2 = \xi_{l,ISI}^2 + \xi_{l,ICI}^2 \tag{4.22}$$

Equation 4.20 has several implementation issues, such as algorithm complexity, numerical instability, and large dynamics of exponential functions, and is therefore not suitable for practical implementations. It does, however, serve as a benchmark to compare the performance of other fusion algorithms more suitable for implementation. Also, it can be used to derive other DF rules.

MRC

For this version, and the following modified and time-reversed MRC rules, the assumption of perfect sensors are used, that is:

$$P(\mathbf{x}^l = \mathbf{1}_K|\mathcal{H}_1^l) = P(\mathbf{x}^l = -\mathbf{1}_K|\mathcal{H}_0^l) = 1 \tag{4.23}$$

Which simplifies equation 4.20 to:

$$\ln\left[\frac{\exp\left(-\frac{||\mathbf{y}^l-\sqrt{p^l}\mathbf{G}^l\mathbf{1}_K||^2}{\sigma_{e,l}^2}\right)}{\exp\left(-\frac{||\mathbf{y}^l+\sqrt{p^l}\mathbf{G}^l\mathbf{1}_K||^2}{\sigma_{e,l}^2}\right)}\right] \propto \mathbb{R}\{(\mathbf{a}_{MRC}^l)^\dagger\mathbf{y}^l\} \triangleq \mathbf{\Gamma}_{MRC}^l \tag{4.24}$$

Where

$$\mathbf{a}_{MRC}^l \triangleq \mathbf{G}^l\mathbf{1}_K \tag{4.25}$$

Where one can write the LLR for the wideband case, $\mathbf{\Gamma}_{MRC}^{l,WB}$, as

$$\mathbf{\Gamma}_{MRC}^{l,WB} = \frac{\sqrt{2}\mathbf{\Gamma}_{MRC}^l}{\sigma_{e,l}||\mathbf{a}_{MRC}^l||} \tag{4.26}$$

Equation 4.25 and 4.26 also holds for the following DF rule, only with the MRC notation changed mMRC. For reasoning described in [16], the performance of $\mathbf{\Gamma}_{MRC}^{l,WB}$ when $N \to \infty$ can be evaluated as:

$$\lim_{N\to\infty}\mathbb{E}\{\mathbf{\Gamma}_{MRC}^{l,WB}|\mathbf{G},\mathbf{x}^l\} = \frac{\sqrt{2N\rho^l}\mathbb{R}\{(\mathbf{1}_K)^t\mathbf{A}^l\mathbf{x}^l\}}{\sigma_{e,l}\sqrt{(\mathbf{1}_K)^t\mathbf{A}^l\mathbf{1}_K}} \tag{4.27}$$

If one models the multipath fading channel on each subcarrier between the SUs an the DFC with the number of channel taps equal to the number of SUs present, and one assumes uncorrelated decision, then equation 4.27 can be simplified to

$$\lim_{N\to\infty} \mathbb{E}\{\mathbf{\Gamma}^{l,WB}_{MRC}|\mathbf{G},\mathbf{x}^l\} = \frac{\sqrt{2N\rho^l}\sum_{k=1}^{K} x_k^l \lambda_k \beta_k^l(k-1)}{\sigma_{e,l}\sqrt{\sum_{k=1}^{K}(\gamma_k\beta_k^l(k-1))^{-1}}} \tag{4.28}$$

Modified MRC (mMRC)

In order to exploit the signal-to-interference-and-noise ratio as it increases with N, one can resort to an alternative form of MRC, namely mMRC. Here, $\mathbf{a}^l_{mMRC}$ becomes

$$\mathbf{a}^l_{mMRC} \triangleq \mathbf{G}^l(\mathbf{A}^l)^{-1}\mathbf{1}_K \tag{4.29}$$

Where $(\mathbf{A}^l)^{-1}$ is a zero-forcing term to remove rule dependence on large-scale fading coefficients as N increases. [16]. The performance evaluation term becomes

$$\lim_{N\to\infty} \mathbb{E}\{\mathbf{\Gamma}^{l,WB}_{mMRC}|\mathbf{G},\mathbf{x}^l\} = \frac{\sqrt{2N\rho^l}\mathbb{R}\{(\mathbf{1}_K)^t\mathbf{x}^l\}}{\sigma_{e,l}\sqrt{(\mathbf{1}_K)^t(\mathbf{A}^l)^{-1}\mathbf{1}_K}} \tag{4.30}$$

Using the same simplifications used for equation 4.28, equation 4.30 becomes

$$\lim_{N\to\infty} \mathbb{E}\{\mathbf{\Gamma}^{l,WB}_{mMRC}|\mathbf{G},\mathbf{x}^l\} = \frac{\sqrt{2N\rho^l}\sum_{k=1}^{K} x_k^l}{\sigma_{e,l}\sqrt{\sum_{k=1}^{K}(\lambda_k\beta_k^l(k-1))^{-1}}} \tag{4.31}$$

Time-Reversal MRC (TR-MRC)

Due to the issues described in section 4.3.7, one can apply a time-reversed approach to the fusion rules. Let

$$\mathbf{a}^l_{TR-MRC} \triangleq \check{\mathbf{G}}^l\mathbf{1}_K \tag{4.32}$$

And thus, the for the wideband case:

$$\mathbf{\Gamma}^{l,WB}_{TR-MRC} = \frac{\sqrt{2}\mathbf{\Gamma}^l_{TR-MRC}}{\sigma_{e,l}||\mathbf{a}^l_{TR-MRC}||} \tag{4.33}$$

The performance evaluation becomes

$$\lim_{N\to\infty} \mathbb{E}\{\mathbf{\Gamma}^{l,WB}_{TR-MRC}|\mathbf{G},\mathbf{x}^l\} = \frac{\sqrt{2N\rho^l}\mathbb{R}\{(\mathbf{1}_K)^t\mathbf{F}^l\mathbf{x}^l\}}{\sigma_{e,l}\sqrt{(\mathbf{1}_K)^t\check{\mathbf{A}}^l\mathbf{1}_K}} \tag{4.34}$$

With the simplifications from equation 4.28, equation 4.34 becomes

$$\lim_{N\to\infty} \mathbb{E}\{\mathbf{\Gamma}^{l,WB}_{TR-MRC}|\mathbf{G},\mathbf{x}^l\} = \frac{\sqrt{2N\rho^l}\sum_{k=1}^{K} x_k^l\lambda_k^l\sqrt{\beta_k^l(K-k)}\sqrt{\beta_k^l(k-1)}}{\sigma_{e,l}\sqrt{\sum_{k=1}^{K}\lambda_k^l\beta_k^l(K-k)}} \tag{4.35}$$

Time-Reversal mMRC (TR-mMRC)

Like in mMRC, the time-reversed version also aims at exploiting linear signal-to-interference-and-noise ratio with $N \to \infty$. Again, similar to equation 4.29, $\mathbf{a}^l_{TR-mMRC}$ can be written as

$$\mathbf{a}^l_{TR-mMRC} \triangleq \check{\mathbf{G}}^l(\check{\mathbf{A}}^l)^{-1}\mathbf{1}_K \tag{4.36}$$

$\mathbf{\Gamma}^{l,WB}_{TR-MRC}$ becomes

$$\mathbf{\Gamma}^{l,WB}_{TR-mMRC} = \frac{\sqrt{2}\mathbf{\Gamma}^l_{TR-mMRC}}{\sigma_{e,l}||\mathbf{a}^l_{TR-mMRC}||} \tag{4.37}$$

And then performance evaluation becomes

$$\lim_{N\to\infty} \mathbb{E}\{\mathbf{\Gamma}^{l,WB}_{TR-mMRC}|\mathbf{G},\mathbf{x}^l\} = \frac{\sqrt{2N\rho^l}\mathbb{R}\{(\mathbf{1}_K)^t(\check{\mathbf{G}}^l)^\dagger((\check{\mathbf{A}}^l)^{-1})^\dagger\mathbf{G}^l\mathbf{x}^l\}}{\sigma_{e,l}\sqrt{(\mathbf{1}_K)^t((\check{\mathbf{A}}^l)^{-1})^\dagger\mathbf{1}_K}} \tag{4.38}$$

Again, with the assumptions used for equation 4.28, 4.38 becomes

$$\lim_{N\to\infty} \mathbb{E}\{\mathbf{\Gamma}^{l,WB}_{TR-mMRC}|\mathbf{G},\mathbf{x}^l\} = \frac{\sqrt{2N\rho^l}\sum_{k=1}^K x^l_k\frac{\sqrt{\beta^l_k(K-k)}}{\sqrt{\beta^l_k(k-1)}}}{\sigma_{e,l}\sqrt{\sum_{k=1}^K(\lambda^l_k\beta^l_k(K-k))^{-1}}} \tag{4.39}$$

4.4 Practical Implementation and Issues

This section will describe the practical aspects of what was done for the experiment setup, such as the programs written to emulate the PU and SUs, as well as modifications done to the NI Massive MIMO framework. The many issues that arose will also be discussed in great detail.

4.4.1 Problems

How the experiment setup was initially envisioned, and what was actually possible in the given time frame, differed significantly, much because of issues that were beyond our control. In the following subsections, these issues will be explained in greater detail.

Envisioned time frame

As the NI MIMO Application Framework was only recently acquired by NTNU, the initial plan from the department was that it would be set up and ready for experiments from the first week of March 2017. Thus, the envisioned schedule at the start of the semester was as follows:

- **Mid January - beginning March**: Study literature related to decision fusion algorithms and other theoretical aspects described in chapter 2

- **Beginning March - Beginning May**: Perform experiment, collect measurements
- **Beginning May - Mid June**: Analyze data, discuss results, finish writing thesis

Delayed MIMO Framework Setup

Due to delays, the MIMO Application Framework was unfortunately not set up until the middle of April, and even then, the department lab engineers still had to perform further tests to assure it was working correctly. Thus, at this point, the schedule was already pushed back one and a half months.

Power Outage

At the end of April, the entire department suffered an unexpected power outage. This had the unfortunate effect of causing most of the framework USRP radios to stop working, which took around a week to fix. Thus, our schedule was pushed back by another week.

Licence Issues

We were given temporary licences to install the LabVIEW Communications MIMO Application Framework on our own computers in order to study the code and the possible configurations. This licence was activated in the beginning of March, with a 45-day validity period. We were of the understanding that this could be renewed once it expired, but this turned out not to be the case, as NTNU had been given a limited amount of licences from NI. The department was very helpful in accommodating us in solving this issue by setting up remote access to a computer that had an active, valid licence. However, this took another two weeks. Thus, we were now into the second week of May, a little over two months after the envisioned start of the experiment phase.

Framework Complexity

As the MIMO Application Framework is a rather new, and quite an expensive product, there is not much information to be found regarding user experiences and community support, as only a few institutions has acquired said product so far. Therefore, it was difficult to know beforehand the difficulty level of making configurations and possible code modifications to customize to a specific experiment setup. As it turns out, it is far from trivial. The VIs for both the base station and mobile station are configurable for certain specific scenarios. However, for scenarios beyond this, such as the one described in section 4.4, one needs to make considerable changes to the source code, often through the FPGA modules. With the very limited time we were given, this was unfortunately not feasible.

USRP Transmit Synchronization

One of the requirements for transmitting the local decisions from the SUs is that they all transmit at the same time. Therefore, very strict synchronization between the USRPs

was necessary. However, this turned out to be more difficult than anticipated. Over-the-air synchronization between several USRPs would firstly be challenging to implement, and would only provide loose synchronization, which would be insufficient. Therefore, external synchronization equipment was needed. However, the radio and antenna lab at NTNU was unfortunately not in possession of any such equipment. The department were willing to include it in their next order of radio equipment, but that it would take at least a month before it would arrive, which would be too late.

4.4.2 PU and SU programs

Despite the problems described in section 4.4.1, the planned implementations were carried out as much as possible. Despite the PU and SU programs described below not being used in the eventual experiment setup, it is the hope of the author that they can be useful for someone wanting to set up a similar experiment at a later time. The implementation files can be seen in the attached folder labview_implementation_files.zip.

PU transmitter program

The PU implementation is designed in such a way that if the PU is silent, nothing is transmitted, whereas if active, a random bit sequence of 1s and 0s are created, then modulated with a BPSK modulation scheme at a carrier frequency specified by a control on the program panel, and finally transmitted through one of the transmit antennas. Figure 4.4 shows the panel of an active PU transmitting at a carrier frequency of 915 MHz and a down-converted power spectrum plot.

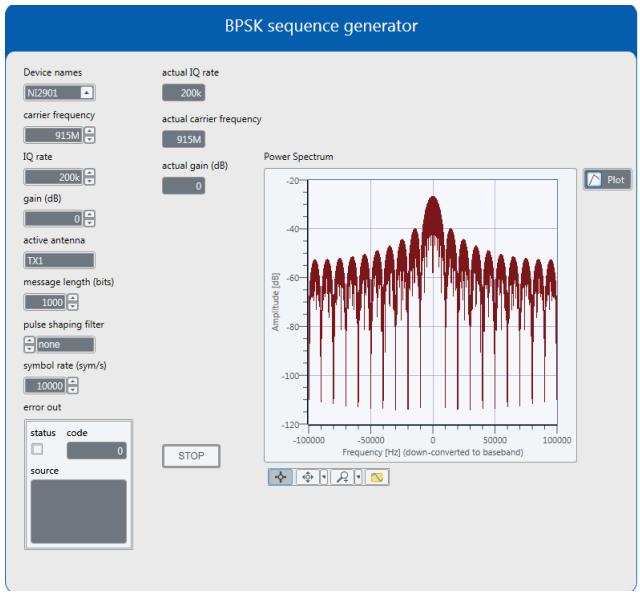

Figure 4.4: PU transmit program panel

SU sensing and transmitting programs

This implementation is designed to iteratively scan a certain spectrum region, each scan containing a center frequency and a certain bandwidth, which should correspond to each sub-band in the WSN model. For each scan, the power spectrum is computed, and the peak power spectrum value is compared to a certain threshold value. A value above this threshold means PU activity, whereas a value below means there is only noise present in the spectrum and therefore means no PU activity. In order to choose this threshold value, one has to take into consideration the propagation environment. As this experiment is meant to take place in an indoor environment, one has to consider the conditions described in section 2.5.1. Figure 4.5 shows the result of scanning the spectrum from 912 MHz to 917 MHz with iterations of 1 MHz and a threshold value of -50 dB, with an active PU running with the configurations shown in figure 4.4.

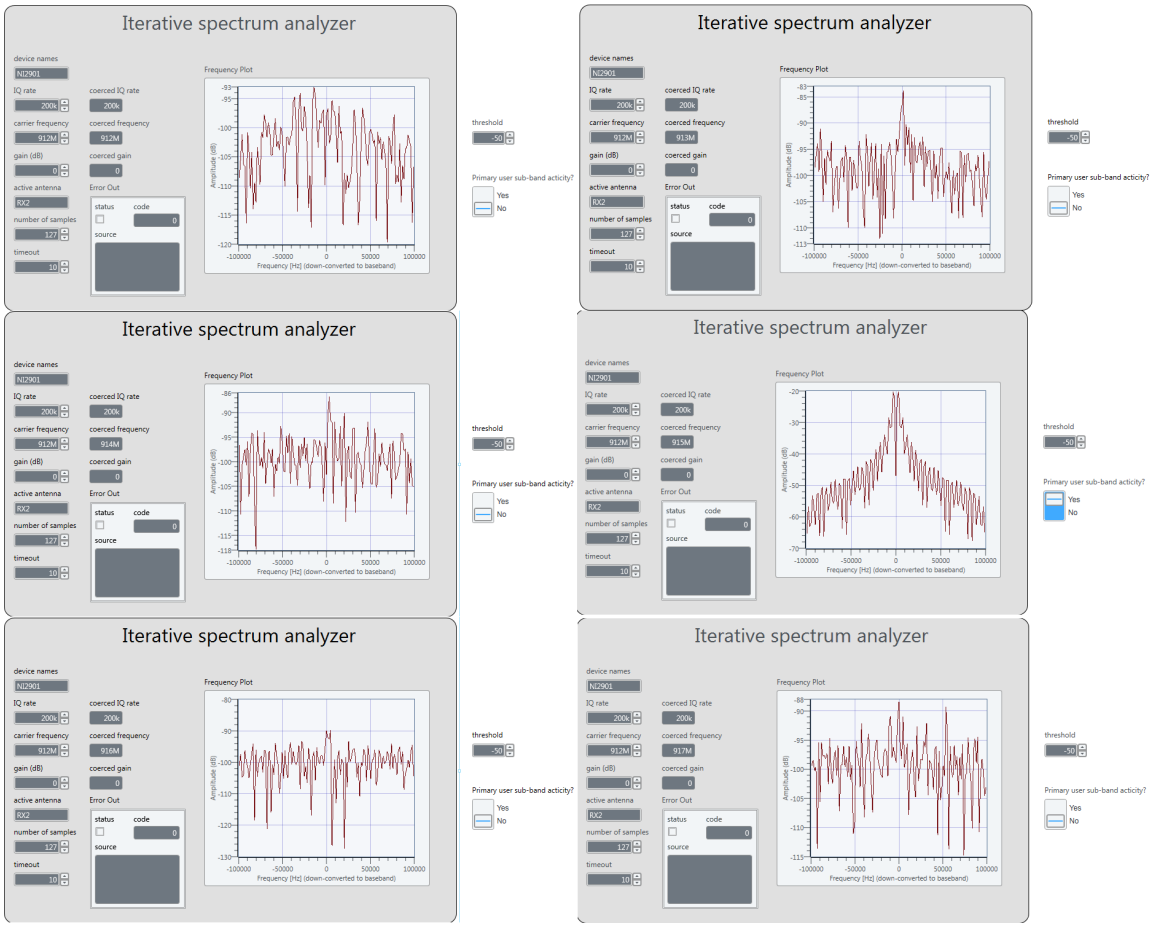

Figure 4.5: SU sensing program panel

As can be seen, the middle-right diagram, with a coerced carrier frequency of 915 MHz,

has a peak power spectrum value of more than 60 dB higher than any of the other scans. As this peak value is above the PU activity threshold, the Boolean PU sub-band activity indicator is switched on.

As for transmitting the local decisions, the plan was to transmit the decisions as one bit on each sub-band to the DFC using a BPSK modulation. However, due to the issues explained in 4.4.1, this was not achievable.

4.4.3 Massive MIMO Framework Overview and Modifications

Simply getting an overview of the framework itself and the significance of the various files was a considerable, time-consuming task. There are vast amounts amounts of various files, each with lots of different modules for tasks such as testbench simulation, FPGA-processing, modulation, channel estimation, etc... There are two main files for configuring the setting for running experiments: the Mobile Station Host, and the Base Station Host. The Base Station Host is meant to be run on the unit controlling the 64-antenna Massive MIMO setup acting as the DFC, whereas the Mobile Station should run on all the units emulating the mobile units, or in our case, SUs. Parts of their respective configuration panels can be seen in figure 4.6 and 4.7, respectively.

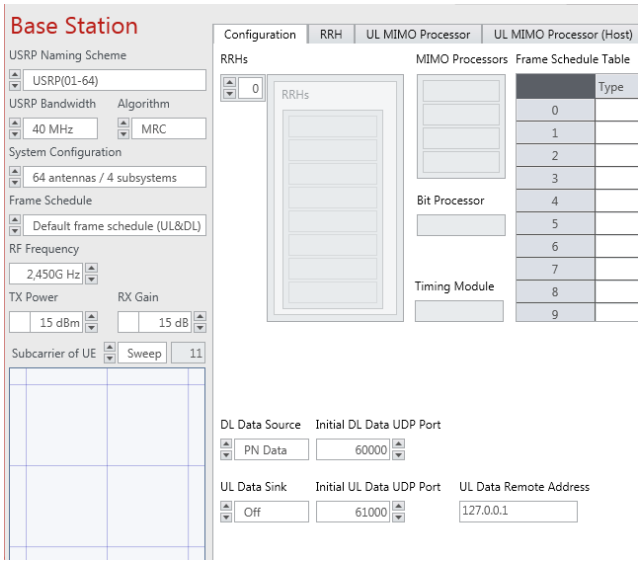

Figure 4.6: Base Station Configuration Panel

LabVIEW Code Modification

As explained in section 4.4.1, getting the mobile units to act as originally envisioned turned out to be too challenging. Therefore, the experiment scenario was reduced to collecting channel measurements between the mobile units acting as the SUs and the Massive MIMO setup acting as the DFC, for these measurements to then eventually be used with the DF

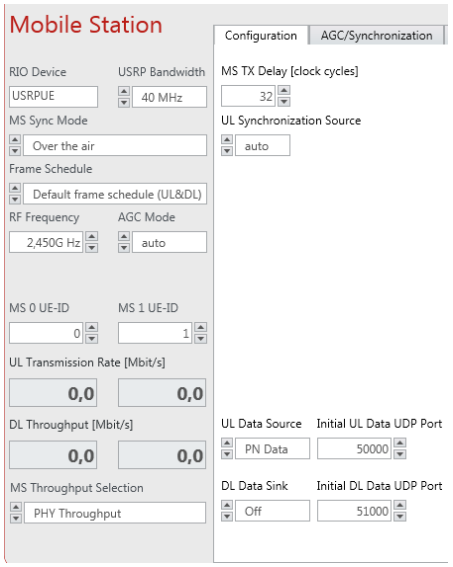

Figure 4.7: Mobile Station Configuration Panel

algorithms in place of the simulated channel data. However, collecting said measurements were not trivial. The Massive MIMO Application Framework does have functionality to calculate properties such as the impulse response, frequency response, and power spectrum for the various channels between the BS and the MS, but said properties are only stored in a temporary data buffer for a few milliseconds before they are discarded. Therefore, in order to save the data to some storage format, one has to make changes to the LabVIEW code in the framework itself. Thus, changes in both the Base Station and Mobile Station .gvi files were made in order to continuously save various types of measurement samples to text files stored locally on the host computers. Snippets of the added code can be seen in Appendix A.

4.5 Experiment Setup

4.5.1 Physical Setup

The experiment was conducted at the circuit and antenna lab at the Department for Electronic Systems at NTNU. Two NI USRP Reconfigurable I/O devices with single-input-single-output (SISO) wireless capabilities, each representing two sensor modules, are used to model the SUs. The 64-antenna Massive MIMO tesbed is as described in section 3.1.3, and is controlled through a mounted PXI chassis and a PC center used for recording and conducting experiments. A block diagram of the setup can be sen in figure 4.8, and figure 4.9 shows how the equipment in the room itself and how the mobile units acting as SUs and the base station acting as the DFC were placed in relation to each other.

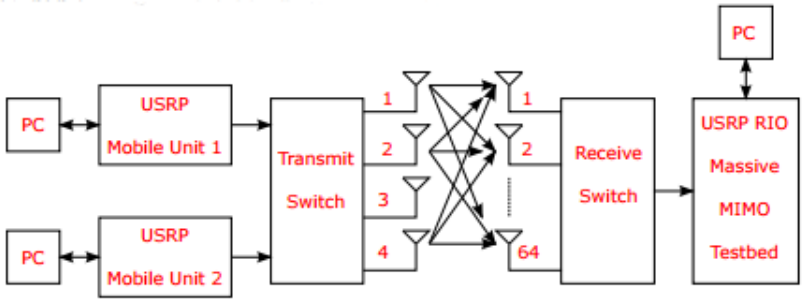

Figure 4.8: Block diagram of experiment setup

4.5.2 System Configuration

The time-varying channel impulse response of 4 x 64 massive MIMO channels with a center frequency of 2.45 GHz with 20 MHz bandwidth and sub-carrier spacing of around 0.18 MHz is measured. The room and the locations of the sensors chosen such that they include interesting scenarios like keyhole effects, both line-of sight and non-line-of-sight communication paths, shadowing due to variety of electrical and laboratory equipment and path loss due to building materials like dry-wall, glass etc. Each measurement set-up is repeated for two main scenarios:

- **Stationary Scenario**: No movement in room
- **Mobile Scenario**: people are continuously moving around in the room.

In both cases, each measurement is recorded for approximately 120 seconds. Due to the channel reciprocity conditions explained in section 2.5.4, it is assumed that channel estimates can be used for both uplink and downlink.

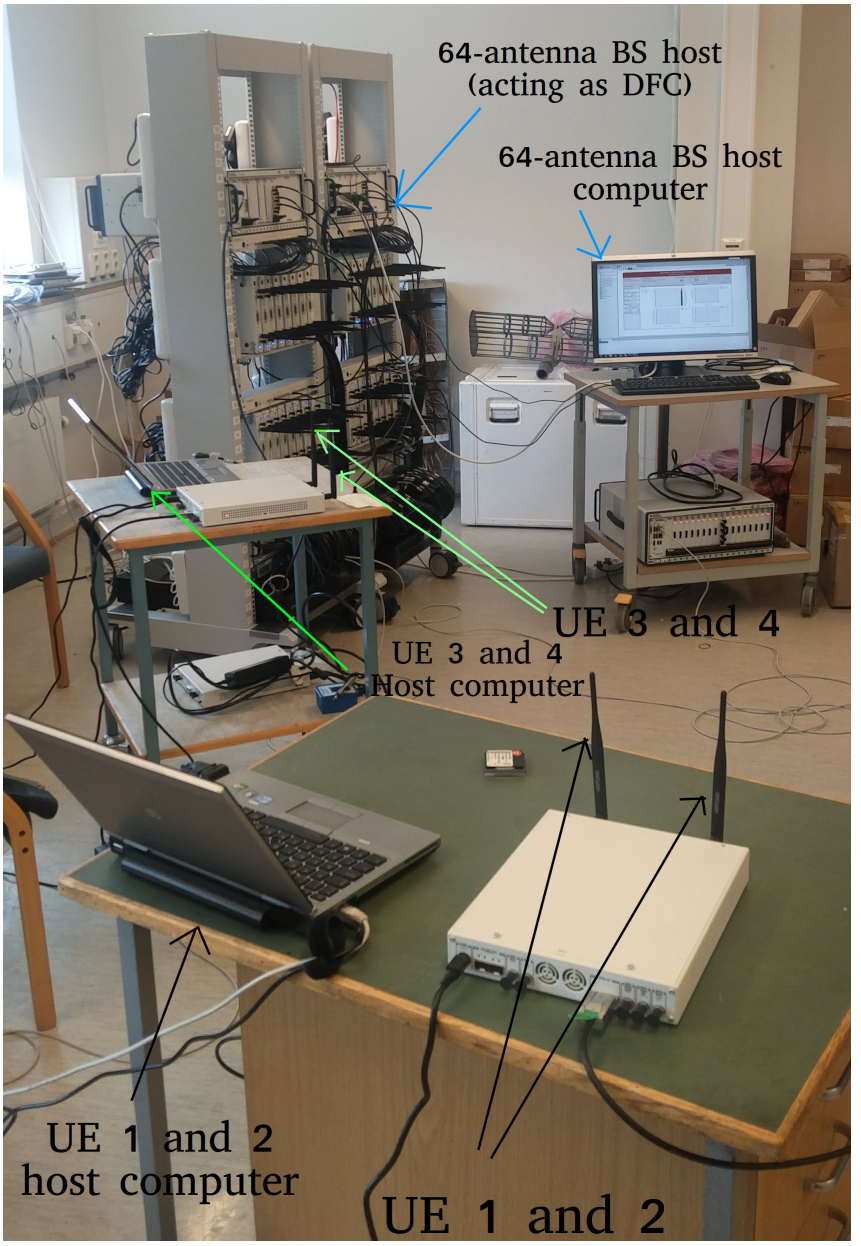

Figure 4.9: Experiment setup in circuit and antenna laboratory

Chapter 5

Results and Discussion

5.1 Simulation

The code for the simulations is based on the signal model, channel model, and DF rules explained in section 4.3, and is written by postdoctoral researcher Indrakshi Dey. Here, the goal is to evaluate the performance of the different MRC rules.

5.1.1 Parameters and assumptions

For simulating the performance, the following assumptions are made:

- The SUs are located in a uniformly random circular area around the DFC with a maximum radius of $r_{max} = 1000$m and a minimum radius of $r_{min} = 100$m.
- The large-scale shadowing is modeled as $\lambda_k^l = \phi_k(\frac{r_{min}}{r_k})^n$, where ϕ_k is a log-normal random variable such that $10\log_{10}(\phi_k) \sim \mathcal{N}(\mu_{\lambda,dB}, \sigma^2_{\lambda,dB})$, where r_k is the distance between the kth SU and the DFC
- For simplicity, let the energy coefficient $\rho^l = \frac{1}{\sqrt{N}}$, and the noise variance $\sigma^2_{w,l} = 1$

5.1.2 ROC Plots and Analysis

Figure 5.1 and 5.2 shows the ROC plots of the resulting simulations, with the TPR, P_{D_0}, as a function of the FPR, P_{F_0}. Each plot shows the performance effect when varying a certain parameter, as explained in the figure captions.

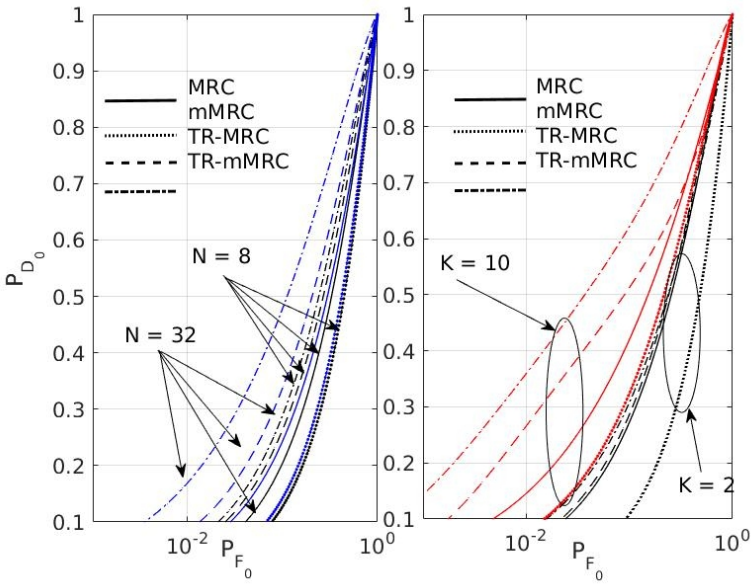

Figure 5.1: ROC plots with varying number of antennas N (left) and varying number of SUs K (right)

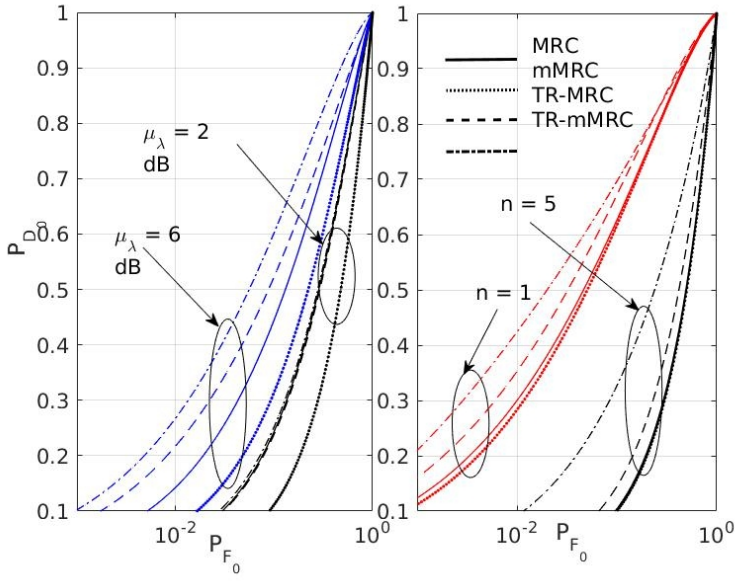

Figure 5.2: ROC plots with varying mean of shadowing effect $\mu_{\lambda,dB}$ (left) and varying path-loss exponent n (right)

Figure 5.1 Evaluation

The following scenario is applied:

- The shadow fading parameters are fixed with $(\mu_{\lambda,dB}, \sigma_{\lambda,dB}) = (4, 2)$
- The path-loss exponent is fixed with $n = 2$.
- For the leftmost figure, the number of SUs is fixed with $K = 8$, whereas the number of antennas, N, is varied.
- For the rightmost figure, the number of antennas is fixed with $N = 32$, whereas the number of SUs, K, is varied.

For the leftmost figure, it seems that mMRC does not outperform MRC, neither for a moderate number of antennas nor a large number of antennas. Also, it appears that increasing the number of antennas does not give a significant performance increase for mMRC. However, it appears that both the time-reversed DF rules, TR-MRC and TR-mMRC outperform their non time-reversed counterparts, with TR-mMRC offering the best performance in both cases.

For the rightmost figure, the two cases of $K = 2$ and $K = 10$ is considered. Like in the leftmost figure, mMRC offers no improvement to the regular MRC. Also, for a small number of SUs, the time-reversed rules offer negligible improvement. However, with a large number of SUs, the time-reversed versions offers considerable improvement over their counterparts, with TR-mMRC again offering the best performance. This large performance increase with large K and TR-MRC/mMRC approach might very well be because of increased spatial diversity and that the channel time reversal combats residual interference.

Figure 5.2 Evaluation

The following scenario is applied:

- Both the number of SUs and antennas are fixed with $(N, K) = (32, 8)$.
- Leftmost figure varies the mean shadowing effect $\mu_{\lambda,dB}$, with $\mu_{\lambda,dB} = 2$ modeling an indoor scenario and $\mu_{\lambda,dB} = 6$ modeling an indoor-to-outdoor scenario. Pathloss exponent is fixed with a value of $n = 2$.
- Rightmost figure varies the path-loss exponent with $n = 1$ being a tunnel-like environment and $n = 5$ being an indoor/outdoor scenario. Mean path loss is fixed at $\mu_{\lambda,dB} = 4$.

For the leftmost figure, when $\mu_{\lambda,dB} = 2$, the time-reversal versions appear unable to combat the shadowing effects, and thus offer very little improvement over the conventional methods. However, when the $\mu_{\lambda,dB}$ increases and the attenuation from the shadowing effect decreases, both time-reversal rules offer significant improvement, with TR-mMRC

coming out as the winner.

For the rightmost figure, both TR-MRC and TR-mMRC offers decent improvement in environments with lower path loss, with TR-mMRC coming out on top. The difference is, however, much clearer in the environment with high path loss as here one can see that TR-mMRC offers clear improvements to both MRC and mMRC, whereas TR-MRC only offers marginal improvement. It should be noted, however, that these results are obtained for both a relatively large K and a large N.

5.2 Data From Massive MIMO Testbed Measurements

This section presents some of the results from the measurements done with the Massive MIMO Testbed Framework at the Circuit and Antenna Lab at NTNU in mid-May.

5.2.1 Measured Scenarios

Recording of the following parameters with a given frame schedule were:

- One active mobile stations acting as SU
  - Frame Schedule: Uplink and Downlink
    - Parameters collected: Channel frequency response between SU and DFC, both for stationary and mobile scenario
- Two active mobile stations acting as SUs
  - Frame Schedule: Uplink and Downlink
    - Parameters collected: Channel frequency response between SUs and DFC, both for stationary and mobile scenario
- Three active mobile stations acting as SUs
  - Frame Schedule: Uplink and Downlink
    - Parameters collected: Channel frequency response between SUs and DFC, both for stationary and mobile scenario
- Four active mobile stations acting as SUs
  - Frame Schedule: Uplink and Downlink, Downlink Only, Uplink Only
    - Parameters collected: Channel frequency response between SUs and DFC, channel impulse response recorded at DFC for all mentioned frame schedules. Transmit Power spectrum recorded at SU for Downlink Only configuration, all done for both stationary and mobile scenario.

As for the other configuration specifics, the following configurations were used at the acting DFC (Base Station.gvi configuration panel):

- **USRP Naming Scheme**: USRP(01-64)
- **USRP Bandwidth**: 40 MHz
- **Algorithm**: MRC
- **System Configuration**: 64 Antennas / 4 Subsystems
- **RF Frequency**: 2.45 GHz
- **USRP Bandwidth**: 40 MHz
- **TX Power**: 15 dBm
- **RX Gain**: 15 dB
- **Data Source**: Pseudorandom Numbers

At the acting SUs (Mobile Station.gvi configuration panels):

- **RIO Device**: USRPUE01/02/03/04
- **USRP Bandwidth**: 40 MHz
- **MS Sync Mode**: Over The Air
- **System Configuration**: 64 Antennas / 4 Subsystems
- **RF Frequency**: 2.45 GHz
- **Data Source**: Pseudorandom Numbers

5.2.2 Data Analysis Considerations

Unfortunately, since this data was recorded at such a late stage in the semester, there was not much time to do much analysis before the thesis deadline, as it is a time-consuming process. A total of 343 megabytes of textfile data was stored in total, and it stands to reason that doing a complete analysis of such a large set of data takes a lot of time. Two of the main steps that have been applied to parts of the data so far in the analysis are:

Measurement Data Start Time: Like previously mentioned, in order to perform the above described measurements the MS nodes and BS node needs to be running simultaneously. However, while the MS nodes get initialized quite quickly once started (at most 10-20 seconds), the BS node usually takes several minutes to initialize all the variables and synchronize with the MS nodes. During this time, the MS nodes are still recording data, which is essentially useless due to there being no active communication channels. Thus, it is necessary to look through the recordings to find at which time the BS and MS get fully synchronized and start transmitting data between each other.

WiFi Interference: Due to lots WiFi access points in the building using frequency bands close to the measurement band of 2.45 GHz, some distortion is to be expected in the

recorded channel impulse response due to random fluctuations of the measurement equipment. Due to this, each recorded measurement snapshot needs to be carefully analyzed to remove distortion and extract clean data.

Applying the above steps to the entire data set is a process that can take up to several months. However, in the section below, results from the analysis of parts of the data set it presented.

5.2.3 Channel Impulse Response plots

While there was not enough time to do a complete data measurement analysis and apply DF rules to compare to the evaluation performance from the simulations presented in section 5.1.2, the initial necessary steps were applied to parts of the measurement collection. The below figures show the plots of the channel impulse responses with four active SUs. Figure 5.3 and 5.4 both have an uplink and downlink frame schedule configuration, with stationary and mobile scenarios, respectively. Figure 5.5 and 5.6 have an uplink-only frame schedule configuration, with stationary and mobile scenarios, respectively.

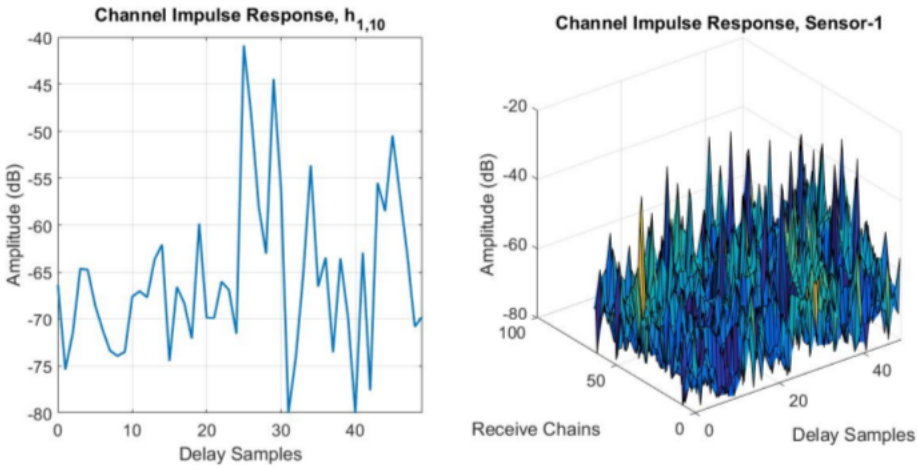

Figure 5.3: *Left*: impulse response between sensor 1 and BS antenna 10. *Right*: Channel impulse response between sensor 1 and all BS antennas

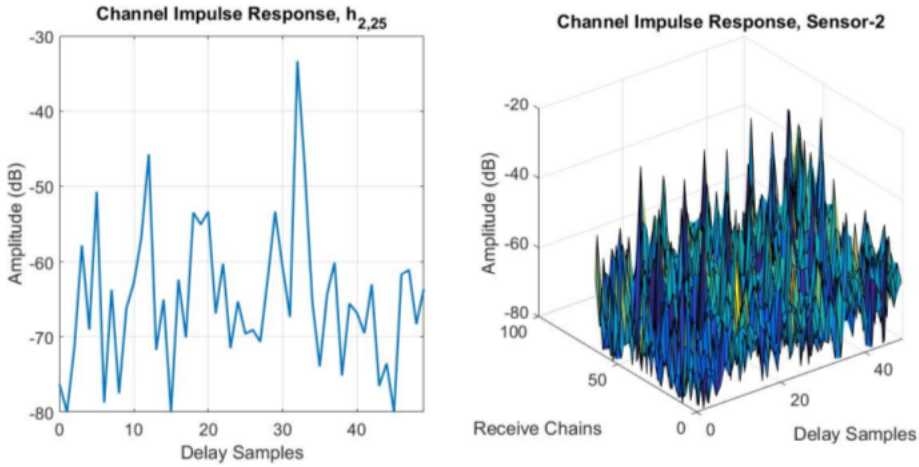

Figure 5.4: *Left*: impulse response between sensor 2 and BS antenna 25. *Right*: Channel impulse response between sensor 2 and all BS antennas

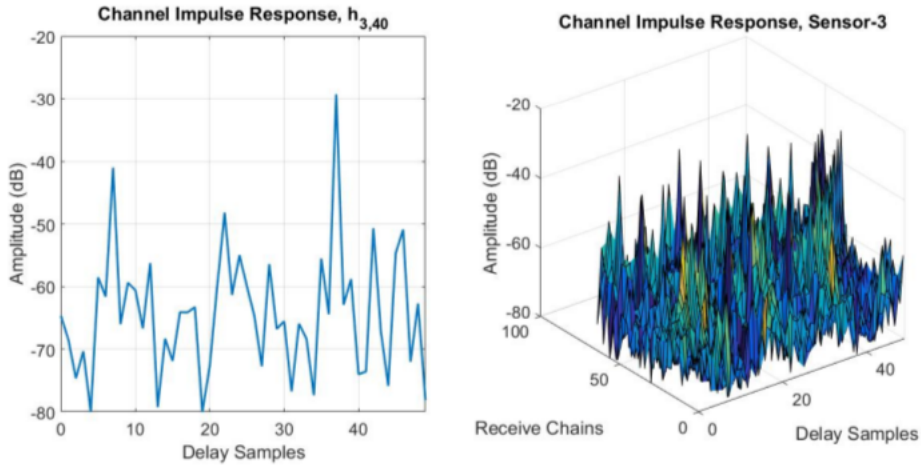

Figure 5.5: *Left*: impulse response between sensor 3 and BS antenna 40. *Right*: Channel impulse response between sensor 3 and all BS antennas

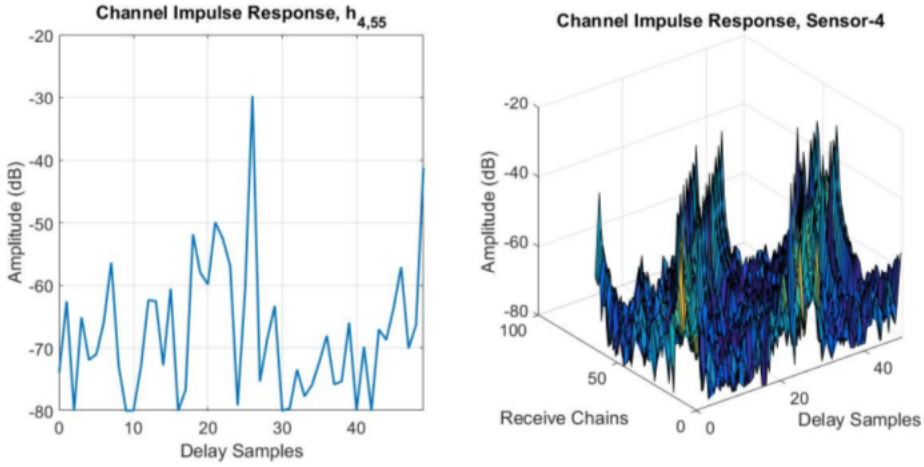

Figure 5.6: *Left*: impulse response between sensor 4 and BS antenna 55. *Right*: Channel impulse response between sensor 4 and all BS antennas

It is difficult to draw any conclusion about the above measurement results, other than at first glance, they seem to have the characteristic impulse response shapes, so it seems that the code added to the framework to record the data did serve its purpose. The next step is to analyze the rest of the data sets in detail and perform comprehensive characterization and performance evaluation. It is the hope that several interesting results will come up from the detailed study of the measured data and will be beneficial for designers of future-generation wireless communication networks.

Chapter 6

Conclusion

6.1 Summary

The main aim of this thesis, in cooperation with post-doctoral researcher Indrakshi Dey, was to explore the practical implications of Massive MIMO Decision Fusion in Wireless Sensor Networks. As the vast majority of the work in this field so far has been purely theoretical with results obtained from simulations, the emphasis here was to use NTNUs newly acquired Massive MIMO testbed framework to obtain real-life results. Thus, an envisioned experiment setup was designed, as described in chapter 4.

The initially envisioned experiment setup, and what was actually possible to accomplish in the given time frame, doesn't exactly match. Due to continuous laboratory setup delays, framework complexity, and various other issues that arose throughout the semester, the experiment was limited to extracting various channel parameters through making modifications to the LabVIEW code in the framework. As the main emphasis of this master thesis is to assist post-doctoral researcher Indrakshi Dey collect measurements for DF analysis to be used in a potential research article, it is the hope of the author that the data that was collected will be of good use. However, data analysis takes time, and as the measurements were done at such a late stage in the semester, the complete analysis is not available at the time of delivery of this thesis.

6.2 Future Work

6.2.1 SU decision transmission program

The LabVIEW code for both the PU transmission program and the SU spectrum sensing program has been written (though not rigorously tested), with emphasis on being easily configurable and designed in such a way that in order to run the latter program on several USRPs acting as SUs, one simply needs to duplicate the files and run them on whichever

terminal controlling the other USRPs. The code for transmitting local decisions for each SU still needs to be written, with two main issues to solve:

- Synchronize the SU USRP radios to sense and transmit at the same time. The best way to do this seems to be through providing all radios with a common synchronization timing source signal provided by an OctoClock from Ettus Research, which is designed specifically for USPR multi-channel synchronization. Having talked to several professors and engineers at the IES department at NTNU, there seems to be a plan to acquire such equipment in the near future
- Configure both the transmission decision signal and Massive MIMO receiver for uplink communication. It was planned to do this during this thesis, but as the synchronization issue was never solved due to lack of equipment, this had to be cut short.

6.2.2 Channel Estimation

The channel parameter estimates were obtained through running both Mobile Station and Base Station nodes on the framework, both of which have built in synchronization and channel estimation mechanisms. The eventual aim is to transmit to the base station nodes from the SU sensing and transmission program outside of the framework. With this scheme, one would need a way to estimate the MIMO communication channel, such as through the use of pilot sequences. A pilot sequence transmission and receiving method would thus have to be implemented at the transmitter and receiver.

6.2.3 DF on the framework

Analyzing the data and performing the DF algorithms is currently envisioned to be done post-processing, that is, all the relevant data is stored in some special format, such as a text file, to be processed at a later time. However, it could be worth to explore whether this could be done directly in real-time on the MIMO Application Framework. This would, however, require extensive knowledge of both communication and low-level electronic design, as modification of many of the framework FPGA modules would probably be necessary. This part alone could be more than enough of a project for an ambitious masters student.

6.3 Closing Remarks

Despite the shortcomings in what was achieved in this thesis compared to the initial experiment setup envisioned at the beginning of the semester, it has been highly interesting to gain insight into and learn more about:

- Massive MIMO Decision Fusion algorithms, which may well play a big role in future wireless sensor networks
- The NI Massive MIMO Application Framework, a state of the art testbed for prototyping future communication systems.

Other than providing measurement data that has the potential to be useful for Next-Generation WSN research, hopefully this thesis can also serve as a good foundation for someone to further build on the presented envisioned system model.

Bibliography

[1] H. B. B. C. M. B. E. M. A. N. S. A. A. D. Paul Harris, Wael Boukley Hasan, "An overview of massive MIMO research at the University of Bristol," 2017.

[2] "Ns2 simulation code for wireless sensor network." https://ns2projects.org/ns2-simulation-code-for-wireless-sensor-network/.

[3] R. Edwards, "802.11ac wireless: Channel bonding, MIMO, spatial streams, and beamforming." https://www.sourceonetechnology.com/802-11ac-wireless-channel-bonding-mimo-spatial-streams-and-beamforming/, 2016.

[4] M. Matthaiou, "MIMO systems in wireless networks." http://www.mehrpouyan.info/MIMO_presentation_Matthaiou.pdf, 2011.

[5] M. Viswanathan, "MIMO diversity and spatial multiplexing." http://www.gaussianwaves.com/2014/08/mimo-diversity-and-spatial-multiplexing/.

[6] M. Khaleel, "Massive MIMO." https://www.slideshare.net/100001290086432/massive-mimo.

[7] "5g massive MIMO testbed: From theory to reality." http://www.ni.com/white-paper/52382/en/, 2017.

[8] L. Frenzel, "Understanding modern digital modulation techniques." http://electronicdesign.com/communications/understanding-modern-digital-modulation-techniques, 2012.

[9] *Enhancement Orthogonal Frequency Division Multiplexing (OFDM) in Wireless Communication Network by Using PTS(Partial Transmit Sequences) Technique*, (Bridgeport, CT, USA), 2014.

[10] V. L. Djamel TEGUIG, Bart SCHEERS, "Consensus algorithms for distributed spectrum sensing based on goodness of fit test in cognitiveradio networks." https://www.researchgate.net/publication/274080097_Consensus_Algorithms_for_Distributed_Spectrum_Sensing_Based_on_Goodness_of_Fit_Test_in_Cognitive_Radio_Networks, 2015.

[11] Y. I. Solimanzoy Fayeqa Haider, Cong Li, "Performance of af relay networks with multiple relays and multiple antennas at destination using mrc combining," *Int'l J. of Communications, Network and System Sciences*, vol. 6, 2013.

[12] W. contributors, "Software-defined radio." https://en.wikipedia.org/wiki/Software-defined_radio, 2017.

[13] S. M. K. Y. Ronald Walpole, Raymond Myers, *Probability & Statistics for Engineers & Scientists*. Upper Saddle River, New Jersey: Pearson Education, 2007.

[14] X. W. Yungag Zhu, Dayou Liu, "Selective and incremental fusion for fuzzy and uncertain data based on probabilistic graphical model," *Journal of Intelligent & Fuzzy Systems*, vol. 29, pp. 2397–2403, 2015.

[15] L. L. P. H. K. N. N. K. I. W. O. E. Steffen Malkowsky, Joao Vieira, "The world's first real-time testbed for massive MIMO: Design, implementation, and validation," *IEEE Access*, 2016.

[16] S. D. Domenico Ciuonzo, Pierluigi Salvo Rossi, "Massive MIMO channel-aware decision fusion," *IEEE TRANSACTIONS ON SIGNAL PROCESSING*, vol. 63, pp. 604–619, 2015.

[17] "What is decision fusion." http://www.igi-global.com/dictionary/decision-fusion/6992.

[18] I. Dey, "Wideband collaborative spectrum sensing using massive MIMO decision fusion." Unpublished research paper, 06 2017.

[19] P. S. R. Domenico Ciuonzo, Gianmarco Romano, "Channel-aware decision fusion in distributed MIMO wireless sensor networks: Decode-and-fuse vs. decode-then-fuse," *IEEE TRANSACTIONS ON WIRELESS COMMUNICATIONS*, vol. 11, pp. 2976–2985, 2012.

[20] "Ni announces world's first application framework for massive MIMO to speed innovation in 5g prototyping." http://www.ni.com/newsroom/release/ni-announces-worlds-first-application-framework-for-massive-mimo-to-speed-innovation-in-5g-prototyping/en/, 2016.

[21] "Bristol and lund set a new world record in 5g wireless spectrum efficiency." http://www.bristol.ac.uk/news/2016/march/massive-mimo.html, 2016.

[22] "What is a wireless sensor network?." http://www.ni.com/white-paper/7142/en/, 2016.

[23] N. M. Gargi Sharma, Mayank Verma, "Analysis of transmission technologies in wireless sensor networks," *International Journal of Engineering Research & Technology*, vol. 3, pp. 2440–2444, 2014.

[24] A. Marcham, "What is massive MIMO?." http://www.cambiumnetworks.com/blog/what-is-massive-mimo/, 2016.

[25] M. Viswanathan, “Introduction to ofdm – orthogonal frequency division multiplexing.” http://www.gaussianwaves.com/2011/05/introduction-to-ofdm-orthogonal-frequency-division-multiplexing/.

[26] *ASPECTS OF FAVORABLE PROPAGATION IN MASSIVE MIMO*, (Linkoping University, Sweden), 2014.

[27] E. Luther, “MIMO application framework white paper.” http://www.ni.com/white-paper/53207/en/, 2016.

[28] C.-X. W. Y. C. Hongjian Sun, Arumugam Nallanathan, “Wideband spectrum sensing for cognitive radio networks: A survey,” *IEEE Access*, 2013.

[29] A. L. S. A. A. R. Z. Lu Lu, Geoffrey Ye Li, “An overview of massive MIMO: Benefits and challenges,” *IEEE Journal of Selected Topics in Signal Processing*, vol. 8, pp. 742–758, 2014.

Appendix LabVIEW Code to Modify Framework

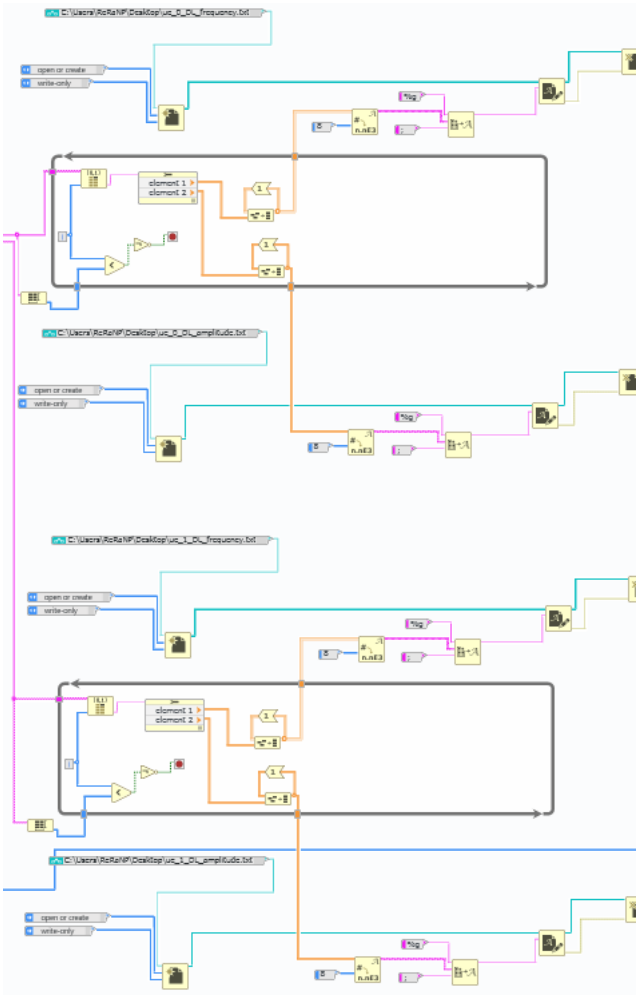

Code snippet in file Mobile Station Host.gvi for storing channel frequency response

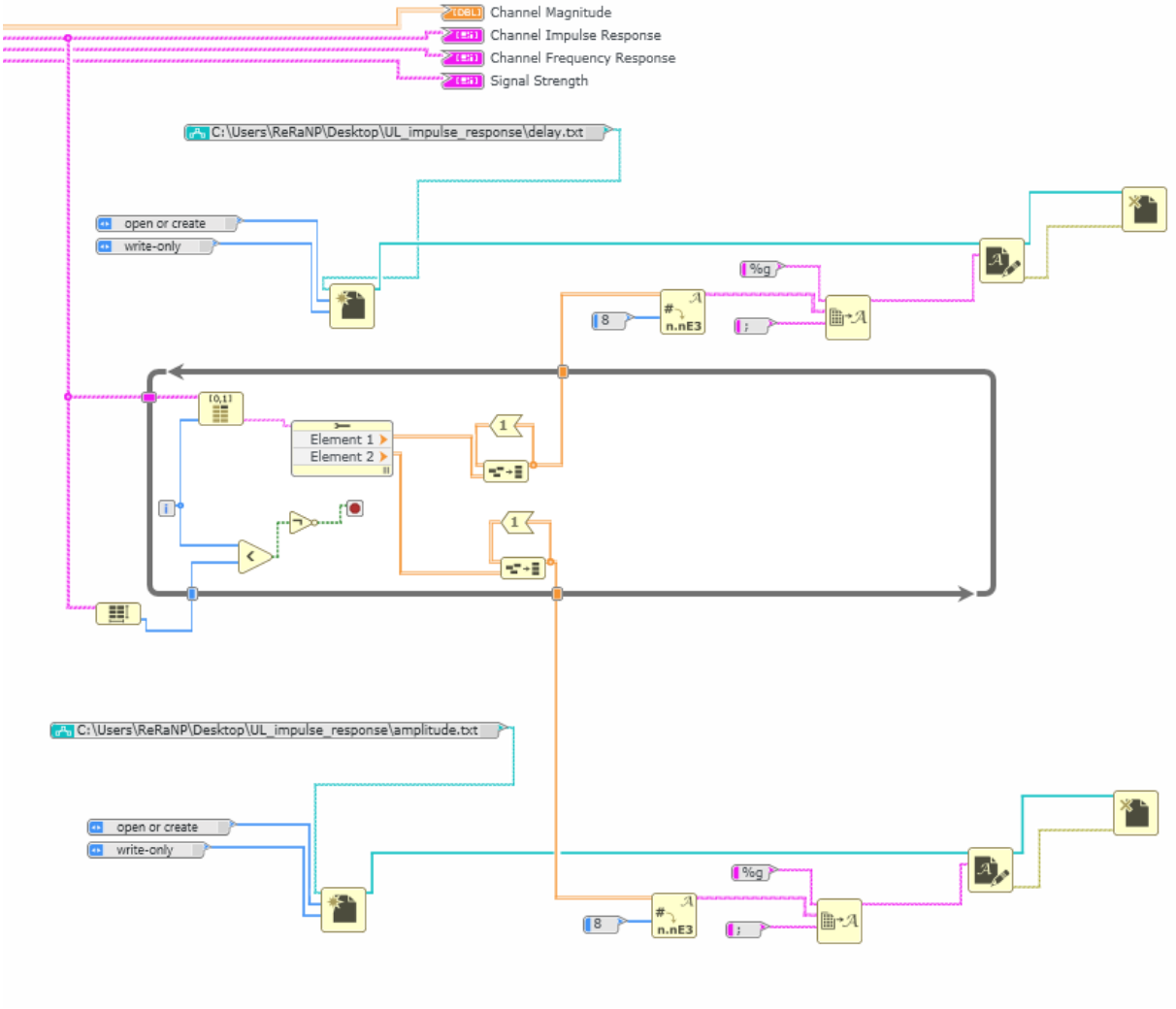

Code snippet in file Base Station Host.gvi for storing channel impulse response

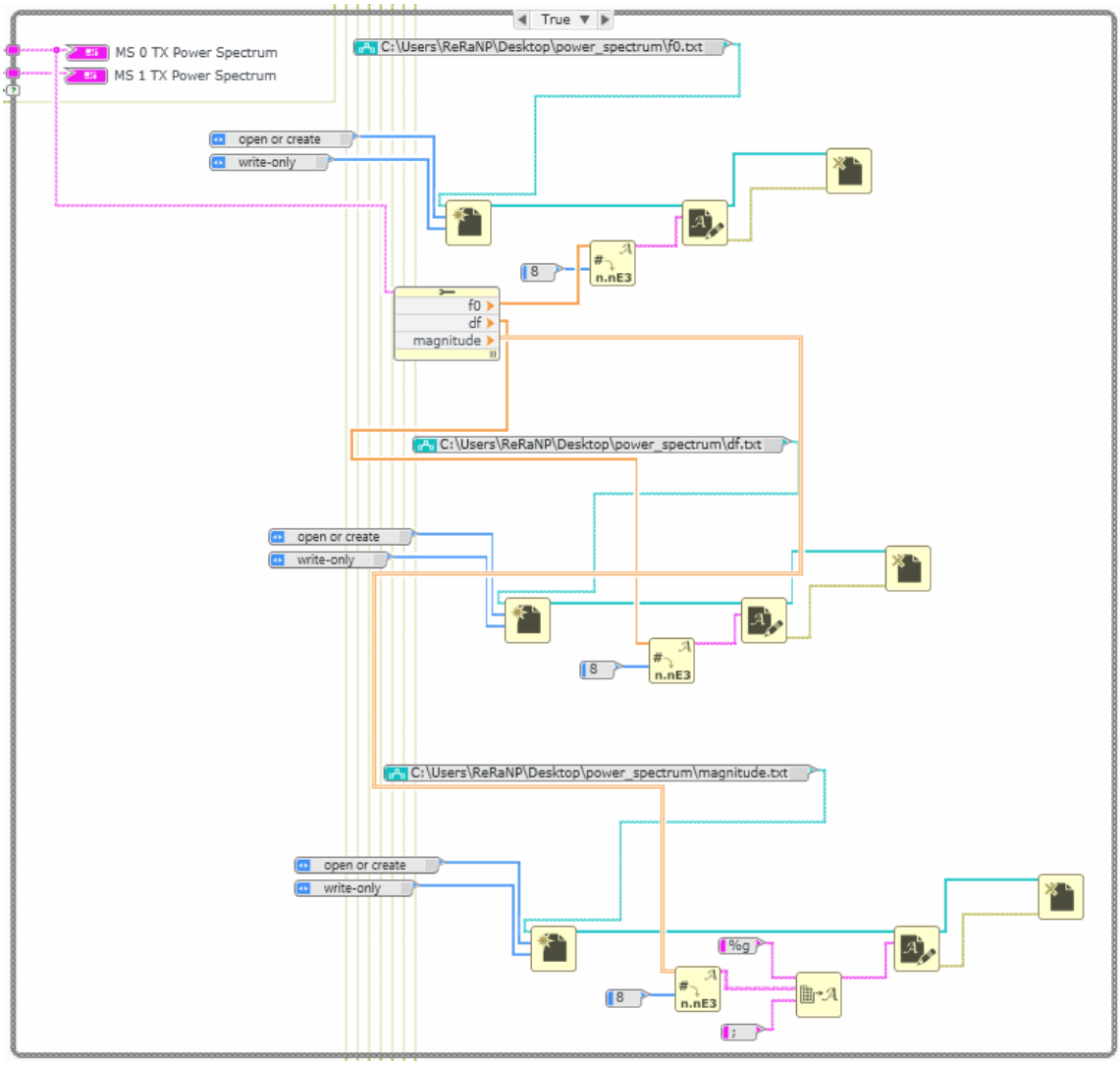

Code snippet in file Mobile Station Host.gvi for storing the transmit power